Multi-Hop Wireless Optical Backhauling for LiFi Attocell Networks: Bandwidth Scheduling and Power Control

Multi-Hop Wireless Optical Backhauling for LiFi Attocell Networks: Bandwidth Scheduling and Power Control

Hossein Kazemi, *Member, IEEE,* Majid Safari, *Member, IEEE,* and Harald Haas, *Fellow, IEEE*

***Abstract*—The backhaul of hundreds of light fidelity (LiFi) base stations (BSs) constitutes a major challenge. Building on an indoor wireless optical backhauling approach, this paper presents the top-down design of a multi-hop wireless backhaul configuration for multi-tier optical attocell networks by proposing super cells. Such cells incorporate multiple clusters of attocells that are connected to the core network via a single gateway. Consequently, new challenges arise for managing the bandwidth and power of the bottleneck backhaul. By putting forward user-based bandwidth scheduling (UBS) and cell-based bandwidth scheduling (CBS) policies, the system-level modeling and analysis of the end-to-end multi-user sum rate is elaborated. In addition, optimal bandwidth scheduling under both UBS and CBS policies are formulated as constrained convex optimization problems, and solved by using the projected subgradient method. Furthermore, the transmission power of the backhaul system is opportunistically reduced using a fixed power control (FPC) strategy. The notion of backhaul bottleneck occurrence (BBO) is introduced. An accurate approximate expression of the probability of BBO is derived, and verified using Monte Carlo simulations. Several insights are provided by studying different aspects of the performance of super cells including the average sum rate, the BBO probability and the backhaul power efficiency (PE).**

***Index Terms*—Light fidelity (LiFi) attocell network, wireless optical backhaul, super cell, multi-hop decode-and-forward (DF) relaying, tree topology, bandwidth scheduling, power control.**

I. Introduction

The advent of light emitting diodes (LEDs) has radically changed the modern lighting industry due to their distinguished features including high energy efficiency, long operational lifetime, a compact form factor, easy maintenance and low cost. The visible light (VL) spectrum offers a vast amount of unregulated bandwidth in 400–790 THz. This unique opportunity is exploited for the deployment of value-added services based on visible light communication (VLC) to piggyback the wireless communication functionality onto the future lighting network in homes/offices [2]. From a network deployment perspective, the dense distribution of indoor luminaires lays the groundwork for establishing ultra-dense light fidelity (LiFi) attocell networks.

This work was financially supported in part by the Engineering and Physical Research Council (EPSRC) under the Established Career Fellowship Grant EP/R007101/1, and in part by the Wolfson Foundation and the Royal Society. This paper was presented in part at the IEEE Global Communications Conference (GLOBECOM), December 2018 [1].

The authors are with the LiFi Research and Development Center (LRDC), Institute for Digital Communications, School of Engineering, The University of Edinburgh, Edinburgh EH9 3FD, UK (email: h.kazemi@ed.ac.uk; majid.safari@ed.ac.uk; h.haas@ed.ac.uk).

Backhaul is an essential part of the cellular network architecture, granting base stations (BSs) access to the core network. Therefore, it is crucial to provide high data rate and reliable backhaul links for transporting the busy wireless traffic between BSs and the core network. Developing cost-effective backhauling solutions for massively deployed small cells is considered as one of the most important challenges in the rollout of the forthcoming 5G cellular networks [3]. To achieve multi-Gbits/s connectivity for indoor broadband wireless networks, a fiber-to-the-home/premises technology based on a passive optical network (PON) architecture is used [4]. For multi-dwelling buildings, signal distribution from the optical fiber hub to individual dwellings is also a major component of the access network. In-building backhauling can be done either wired or wirelessly. To this end, wired solutions based on Ethernet and power line communication (PLC) have been considered [5], [6]. In addition, it is possible to realize the distribution network within buildings wirelessly using millimeter wave (mmWave) communications in the 60 GHz band, which has been found suitable for indoor environments [7]. An efficient alternative to complement fiber-based PON, namely G.fast, has been standardized [8], which is a high speed digital subscriber line technology promising Gbits/s connectivity over copper wires for distances up to 250 m.

When it comes to densely deployed optical attocell networks, because of the sophisticated structure of backhaul connections for multiple LiFi BSs, designing an efficient backhaul network is more challenging. Prior studies have addressed the problem of backhauling for indoor VLC systems by three main approaches: employing PLC to reach light fixtures through the existing electricity wiring infrastructure in buildings, thus creating hybrid PLC-VLC systems [9]–[12]; interfacing Ethernet technology with VLC that allows the distribution of both data and electricity to LED luminaires by a single Category 5 cable based on the Power-over-Ethernet standard [13], [14]; and extending single mode optical fiber cables to LED lamps to enable multi-Gbits/s connectivity based on an integrated PON-VLC architecture [15]–[17].

As an alternative to the aforementioned approaches, backhauling for indoor LiFi networks can be designed based on wireless optical communications. In particular, the idea of using VLC to build inter-BS links in optical attocell networks with a star topology was first put forward in [18]. The work in [19] carried out an extended design and optimization of the wireless optical backhaul system in both VL and infrared (IR) bands by using a tree topology. In these works, the

bandwidth of the shared backhaul was assumed to be equally apportioned among multiple downlink paths. The study in [1] proposed heuristic methods for bandwidth scheduling in a two-tier LiFi network, and introduced new criteria to control the total power of the backhaul system. However, the problem of optimal bandwidth scheduling remains unexplored. Furthermore, although preliminary results for power control and backhaul bottleneck performance were presented in [1], an in-depth analysis of such new aspects is subject to an extended study.

This paper primarily attempts to address the above-mentioned shortcomings by putting forward the design and analysis of multi-hop wireless optical backhauling for multi-tier optical attocell networks through the introduction of the novel concept of super cells. Note that this is not a trivial extension due to the intricate configuration of a multi-tier multi-hop super cell. Furthermore, this work makes multiple contributions including:

- Novel user-based bandwidth scheduling (UBS) and cell-based bandwidth scheduling (CBS) policies are proposed for dividing the shared bandwidth of the backhaul system.
- The end-to-end multi-user sum rate is derived for the generalized case of multi-tier super cells for both UBS and CBS policies, by employing direct current-biased optical orthogonal frequency division multiplexing (DCO-OFDM) and decode-and-forward (DF) relaying.
- For each policy, the optimal bandwidth allocation is formulated as an optimization problem and novel optimal bandwidth scheduling algorithms are developed.
- A fixed power control (FPC) mechanism is proposed to set a controlled operating point for the total backhaul power. Concerning the access system performance, three main schemes are devised: maximum SINR power control (MSPC), average SINR power control (ASPC) and average rate power control (ARPC). For each scheme, the corresponding power control coefficient is derived in closed form.
- The notion of backhaul bottleneck occurrence (BBO) is scrutinized by a thorough analysis and a tight approximation of the BBO probability is derived analytically.
- New insights are provided into the performance of multi-tier super cells by studying the average sum rate, the BBO probability and the backhaul power efficiency (PE).

A longer version of this paper with more discussions in some parts including the proof of Lemma 4 is available in the preprint manuscript [20].

II. Multi-Hop Wireless Backhaul System Design

This section presents system-level principles and preliminaries required for the design and analysis of a multi-hop wireless optical backhaul network using a top-down approach.

A. Network Configuration and Super Cells

In this paper, an unbounded optical attocell network with a hexagonal tessellation is considered. Such a model is appropriate for network deployments in spacious office environments [21]. The network incorporates multi-tier bundles of hexagonal attocells which are referred to as *super cells* in this work, with each bundle encompassing one, two or possibly several tiers. The entire network coverage is then *tiled* by multiple super cells. Within every super cell, only the central BS is directly connected to the gateway while the remaining BSs are routed to the gateway using a tree topology that extends from a root at the central BS toward the outer tiers. Here, a tree topology is used for a number of reasons: 1) It guarantees the shortest path between the gateway and every BS in any tier of the network; 2) It is well matched with the hexagonal cellular layout due to a circular symmetry of the network around the central BS; and 3) It can be scaled for multi-tier networks based on the proposed super cell structure. Let N_{T} denote the total number of tiers deployed. For clarity, one branch of a super cell with $N_{\mathrm{T}} = 5$ is illustrated in Fig. 1[1]. A wireless optical communication technology operating in the IR optical band [22] is employed to establish inter-BS backhaul links. The use of the IR band allows to cancel unwanted backhaul-induced interference on the VL access network [18]. Besides, wireless IR communication has advantages that makes it preferable over VLC for the backhaul system design, mainly including the availability of a wider modulation bandwidth.

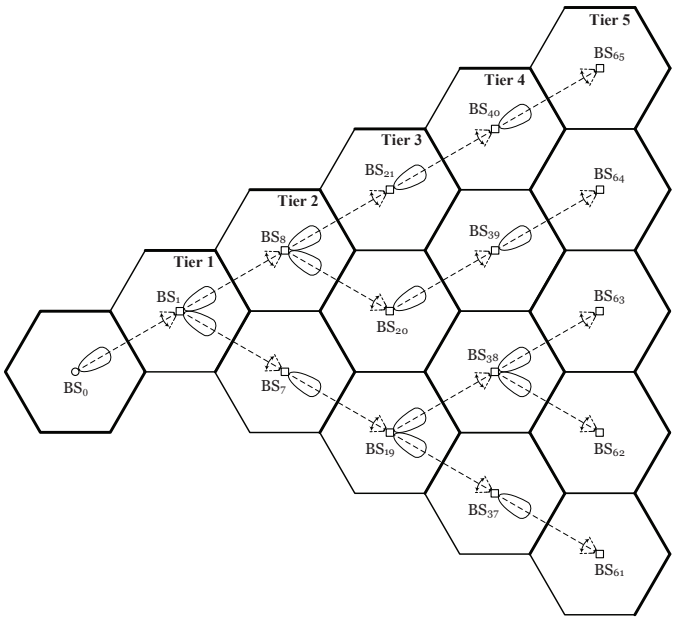

Fig. 1: One branch of a five-tier super cell with multi-hop wireless optical backhaul links.

In contrast to white LEDs whose emitted optical power is distributed over a broad spectrum in the 380–880 nm VL region, commercial, inexpensive IR LEDs emits invisible, monochromatic light with peak wavelengths at 850 nm or 950 nm depending upon the chemical compound used. In addition, their output light is of much narrower linewidth compared with white LEDs, with a spectral bandwidth of about 40–50

[1]The super cell picture is completed by rotating and repeating the shown branch every 60° counterclockwise. Nevertheless, this is just an illustration and the generality of presentation is maintained throughout the paper by adopting a parametric modeling methodology, i.e. for a general case of the kth branch for $k = 1, 2, \ldots, 6$.

nm. The practical implication of these specifications is that multipath reflections in the wireless IR channel are received with a magnitude larger than those in the VL channel because the indoor materials exhibit higher reflectance in the IR band [23]. Nevertheless, this effect is not significant as long as LEDs with a highly directive emission profile are used. In practice, an efficient concentration of light for IR LEDs is attained by using embedded optical lenses. Furthermore, the switching speed of LEDs is primarily limited by the radiative recombination lifetime of minority carries. Current technologies render the production of highly efficient IR LEDs feasible, yielding 3-dB cutoff frequencies in excess of 100 MHz, while for off-the-shelf white LEDs, modulation bandwidth is typically about 20 MHz when blue filtering is applied at the receiver.

For the multi-hop wireless optical backhaul system under consideration, by using a sufficiently narrow optical beam and a directed line-of-sight (LOS) configuration, the crosstalk among backhaul links is effectively canceled [19]. Hence, BSs are permitted to perform full duplex relaying to avoid unnecessary loss in the system spectral efficiency (SE). The employment of DCO-OFDM for data transmission in both access and backhaul systems allows efficient management of network resources. In the following, an $N_{\rm a}$-point (resp. $N_{\rm b}$-point) inverse fast Fourier transform (IFFT)/fast Fourier transform (FFT) is used for DCO-OFDM transmission in the access (resp. backhaul) system. The rest of the assumptions are similar to those used in [19].

B. Signal-to-Noise-plus-Interference Ratio

1) Downlink SINR Statistics: A number of user equipment (UE) devices are randomly scattered in the coverage of a super cell with a uniform distribution, attempting to obtain a downlink connection from optical BSs. The downlink channel follows a LOS light propagation model[2]. With the assumption of the whole bandwidth being fully reused across all attocells, the downlink quality in each attocell is influenced by co-channel interference (CCI) from neighboring BSs. The aggregate effect of the received CCI signals is commonly treated as a white Gaussian noise. The received signal is also perturbed by an additive noise comprising signal-independent shot noise and thermal noise. This noise is modeled by a zero mean Gaussian distribution with a single-sided power spectral density (PSD) of N_0.

According to a polar coordinate system with BS_0 at the origin, the electrical signal-to-noise-plus-interference ratio (SINR) per subcarrier for the uth UE associated with BS_i at $z_u = (r_u, \theta_u)$ is given by [21]:

$$\gamma_u = \frac{\xi_{\rm a}^{-1}(r_i^2(z_u)+h^2)^{-m-3}}{\sum\limits_{j\in\mathcal{J}_i}(r_j^2(z_u)+h^2)^{-m-3}+\Omega}, \tag{1}$$

where $\xi_{\rm a} = \frac{N_{\rm a}-2}{N_{\rm a}}$ is the subcarrier utilization factor; $r_i(z_u)$ indicates the horizontal distance of z_u from BS_i; h is the vertical separation between the BS plane (the horizontal plane on which the BSs are located) and the receiver plane (the horizontal plane where the UEs are present); $m = -\frac{\ln 2}{\ln(\cos\Phi_{\rm a})}$ is the Lambertian order and $\Phi_{\rm a}$ is the half-power semi-angle of the downlink LEDs; and $\mathcal{J}_i$ denotes the index set of the interfering BSs for BS_i. In (1), Ω is given by:

$$\Omega = \frac{4\pi^2 N_0 B_{\rm a}\xi_{\rm a}}{\left((m+1)h^{m+1}A_{\rm PD}R_{\rm PD}\right)^2 P_{\rm a}}, \tag{2}$$

where $B_{\rm a}$ is the bandwidth of the access system[3]; $A_{\rm PD}$ is the photosensitive area of photodiode (PD); $R_{\rm PD}$ is the PD responsivity; and $P_{\rm a}$ is the transmission power used for every BS.

The downlink SINR is a random variable through a transformation of the random coordinates of the UE. For an unbounded hexagonal attocell network, the cumulative distribution function (CDF) of the downlink SINR is presented in [21]. A similar methodology is adopted to derive an analytical expression for the CDF of γ_u in (1) as follows:

$$\mathbb{P}\left[\gamma_u \le \gamma\right] = \frac{1}{2} - \frac{2}{\pi R_{\rm e}^2}\int_0^{R_{\rm e}} \arcsin^{\dagger}\left(\mathcal{Z}(r,\gamma)\right) r dr, \tag{3}$$

where $R_{\rm e}$ represents the radius of an equivalent circular cell preserving the area of the hexagonal cell with radius R; and:

$$\mathcal{Z}(r,\gamma) = \frac{2\gamma^{-1}\xi_{\rm a}^{-1}(r^2+h^2)^{-m-3} - 2\Omega}{|\mathcal{I}_{0^\circ}(r) - \mathcal{I}_{30^\circ}(r)|} - \frac{\mathcal{I}_{0^\circ}(r)+\mathcal{I}_{30^\circ}(r)}{|\mathcal{I}_{0^\circ}(r) - \mathcal{I}_{30^\circ}(r)|}, \tag{4}$$

$$\arcsin^{\dagger}(x) = \begin{cases} \frac{\pi}{2}, & x > 1 \\ \arcsin(x), & |x| \le 1 \\ -\frac{\pi}{2}, & x < -1 \end{cases}. \tag{5}$$

The functions $\mathcal{I}_{0^\circ}(r)$ and $\mathcal{I}_{30^\circ}(r)$ appearing in (4) are available in closed form in [21]. Based on (3), the CDF of γ_u is efficiently computed by using numerical integration methods. Note that γ_u is a bounded random variable such that:

$$\gamma_{\min} \le \gamma_u \le \gamma_{\max}, \tag{6a}$$

$$\gamma_{\min} = \frac{\xi_{\rm a}^{-1}(R_{\rm e}^2+h^2)^{-m-3}}{\mathcal{I}_{30^\circ}(R_{\rm e})+\Omega}, \tag{6b}$$

$$\gamma_{\max} = \frac{\xi_{\rm a}^{-1}h^{-2m-6}}{\mathcal{I}_{0^\circ}(0)+\Omega}. \tag{6c}$$

2) Backhaul Signal-to-Noise-Ratio: For IR links operating in the presence of intense ambient light a shot noise is generated that limits the receiver performance [22]. In indoor environments, IR interference commonly arises from artificial light sources such as fluorescent lamps. The detected noise spectrum contains energy up to a few hundreds of kHz [22], so it can be eliminated by high-pass filtering. Specifically, based on DCO-OFDM, the IR system can be made immune to this type of interference by choosing the frequency of the first subcarrier to be sufficiently greater than the effective bandwidth of the interference. Other potential IR sources can still contribute to shot noise, which need to be taken into

[2]Except small regions in proximity to the network boundaries where the non-line-of-sight (NLOS) effect is manifested most, in the rest of areas under coverage, more than 90% of the received optical power comes solely from the LOS component [21].

[3]The LiFi access system is assumed to have a low-pass and flat frequency response with a bandwidth of $B_{\rm a}$.

account. This is included within a single noise term in the received signal, accounting for the aggregate effect of both signal-independent shot noise and thermal noise. In effect, because of having an equal link distance, backhaul links exhibit an identical signal-to-noise ratio (SNR)[4]. The received SNR per subcarrier for the backhaul link of BS_i, denoted by b_i, is [19]:

$$\gamma_{\mathrm{b}_i} = K_i \gamma_{\mathrm{b}}, \tag{7a}$$

$$\gamma_{\mathrm{b}} = \frac{((\ell+1) A_{\mathrm{PD}} R_{\mathrm{PD}})^2 P_{\mathrm{a}}}{36\pi^2 R^4 N_0 B_{\mathrm{b}} \xi_{\mathrm{b}}^2}, \tag{7b}$$

where $K_i = \frac{P_{\mathrm{b}_i}}{P_{\mathrm{a}}}$ is the power control coefficient for the link b_i, and P_{b_i} is the corresponding transmission power; $\ell = -\frac{\ln 2}{\ln(\cos \Phi_{\mathrm{b}})}$ is the Lambertian order with Φ_{b} denoting the half-power semi-angle of the backhaul LEDs; B_{b} is the bandwidth of the backhaul system; and $\xi_{\mathrm{b}} = \frac{N_{\mathrm{b}}-2}{N_{\mathrm{b}}}$.

C. Achievable Rates of Access and Backhaul Systems

The subchannel bandwidths of access and backhaul systems are matched so that $\frac{B_{\mathrm{a}}}{N_{\mathrm{a}}} = \frac{B_{\mathrm{b}}}{N_{\mathrm{b}}}$. This leads to the same symbol periods for DCO-OFDM frames of the two systems. Let $\mathcal{L}_i$ be the index set of BSs whose connection path from the gateway includes the link b_i and let $\mathcal{U}_i$ be the index set of UEs associated with BS_i such that $|\mathcal{U}_i| = M_i$, where $|\ |$ denotes the cardinality of a set. Every UE served by BS_i acquires an equal bandwidth. Furthermore, let $\mathcal{R}_{\mathrm{a}_i}$ be the access sum rate for BS_i and let $\mathcal{R}_{\mathrm{b}_i}$ be the overall achievable rate of b_i. It follows that:

$$\mathcal{R}_{\mathrm{a}_i} = \frac{\xi_{\mathrm{a}} B_{\mathrm{a}}}{M_i} \sum_{u \in \mathcal{U}_i} \log_2(1+\gamma_u), \tag{8a}$$

$$\mathcal{R}_{\mathrm{b}_i} = \xi_{\mathrm{b}} B_{\mathrm{b}} \log_2(1+\gamma_{\mathrm{b}_i}). \tag{8b}$$

D. Decode-and-Forward Relaying and Backhaul Bandwidth Sharing

In an N_{T}-tier super cell, the nth tier encompasses $\frac{6n}{6} = n$ BSs for each branch so that $|\mathcal{T}_n| = n$ for $n = 1, 2, \ldots, N_{\mathrm{T}}$, where $\mathcal{T}_n$ is the index set of BSs in the nth tier. Therefore, the total number of BSs per branch excluding the central BS is calculated by:

$$N_{\mathrm{BS}} = \sum_{n=1}^{N_{\mathrm{T}}} n = \frac{N_{\mathrm{T}}\left(N_{\mathrm{T}}+1\right)}{2}. \tag{9}$$

For the kth branch of the backhaul network, the downlink data traffic for all N_{BS} BSs is carried by the link between the gateway and the first tier, i.e. b_k for some $k \in \mathcal{T}_1$. This requires sufficient capacity for b_k to respond to the aggregate sum rate of all N_{BS} BSs. However, such a challenging requirement is not always possible to be fulfilled in realistic scenarios where the limited capacity of b_k may result in a *backhaul bottleneck*. In this paper, the link b_k $\forall k \in \mathcal{T}_1$ is generally referred to as a *bottleneck link*.

The use of DCO-OFDM in conjunction with DF relaying allows data multiplexing to be realized in the frequency domain. This way, the bandwidth of the bottleneck link b_k is divided into N_{BS} orthogonal sub-bands, with each sub-band allocated to an independent data flow. The symbols encapsulated in different sub-bands are individually and fully decoded at BS_i in the first tier, which thereafter are reassembled into N_{BS} distinct groups. One group alone is modulated with a DCO-OFDM frame and directly transmitted for the downlink of BS_i. The remaining $N_{\mathrm{BS}}-1$ groups are repackaged into separate DCO-OFDM frames and forwarded in their desired directions toward higher tiers. The orthogonal decomposition of the effective bandwidth $\xi_{\mathrm{b}} B_{\mathrm{b}}$ into N_{BS} parts entails a weight coefficient $\mu_i \in [0,1]$ satisfying $\sum_{i \in \mathcal{L}_k} \mu_i = 1$, thereby allocating a dedicated share of $\mu_i \xi_{\mathrm{b}} B_{\mathrm{b}}$ to BS_i $\forall i \in \mathcal{L}_k$.

[4]The wireless optical backhaul system operates over a frequency-flat channel dominated by the LOS path.

III. End-to-End Sum Rate Analysis

The *end-to-end sum rate* refers to the sum of the end-to-end rates of individual UEs. In this paper, two main policies are proposed for bandwidth allocation: UBS and CBS. The end-to-end sum rate under both policies are derived in the following.

A. User-based Bandwidth Scheduling

After performing bandwidth sharing, an independent pipeline is created to transport data from the gateway to every BS. In UBS, the dedicated portion of the backhaul bandwidth and the bandwidth of the access system are equally allocated to UEs for each BS. The end-to-end rate of each UE cannot be greater than the allocated capacity of each intermediate hop based on the maximum flow–minimum cut theorem [24]. Also, bandwidth sharing introduces a loss factor of μ_i into the end-to-end SE of every UE. For BS_i $\forall i \in \mathcal{T}_1$, the uth UE $\forall u \in \mathcal{U}_i$ experiences an end-to-end rate of:

$$\begin{aligned}\mathcal{R}_u^{\mathrm{UBS}} &= \min\left[\frac{\mu_i \xi_{\mathrm{b}} B_{\mathrm{b}}}{M_i}\log_2(1+\gamma_{\mathrm{b}_i}), \frac{\xi_{\mathrm{a}} B_{\mathrm{a}}}{M_i}\log_2(1+\gamma_u)\right], \\ &= \frac{\xi_{\mathrm{a}} B_{\mathrm{a}}}{M_i}\min\left[\mu_i \zeta \log_2(1+\gamma_{\mathrm{b}_i}), \log_2(1+\gamma_u)\right],\end{aligned} \tag{10}$$

where ζ is defined as the effective bandwidth ratio:

$$\zeta = \frac{\xi_{\mathrm{b}} B_{\mathrm{b}}}{\xi_{\mathrm{a}} B_{\mathrm{a}}}. \tag{11}$$

To extend the analysis for the nth tier, note that the signals intended for BSs in the nth tier need to traverse exactly n intermediate hops through backhaul links. Let $\mathcal{P}_i = \{j_1, j_2, \ldots, j_n\}$ denote the path from the gateway to BS_i for some $i \in \mathcal{T}_n$. The elements of $\mathcal{P}_i$ specify the indexes of backhaul links on the way to BS_i, among which j_1 indicates the bottleneck link. For example, $\mathcal{P}_{20} = \{1, 8, 20\}$ according to Fig. 1. Let $\mu_{i,j}$ be the bandwidth sharing ratio that is allocated to BS_i at b_j. To be consistent with the notation used for the first tier, $\mu_{i,j} = \mu_i$ for $j = j_1$. Obviously, $\mu_{i,j_{N_{\mathrm{T}}}} = 1$. Therefore, for BS_i in the nth tier, the end-to-end rate of the uth UE is written in a compact form:

$$\mathcal{R}_u^{\mathrm{UBS}} = \frac{\xi_{\mathrm{a}} B_{\mathrm{a}}}{M_i}\min\left[\min_{j \in \mathcal{P}_i} \mu_{i,j}\zeta \log_2(1+\gamma_{\mathrm{b}_j}), \log_2(1+\gamma_u)\right]. \tag{12}$$

$$\underset{\{\mu_i \in \mathbb{R}\}}{\text{maximize}} \quad \sum_{i\in\mathcal{L}_k}\sum_{u\in\mathcal{U}_i} \frac{\xi_{\mathrm{a}} B_{\mathrm{a}}}{M_i} \min\left[\mu_i \zeta \log_2(1+\gamma_{\mathrm{b}_k}), \log_2(1+\gamma_u)\right] \tag{21a}$$

$$\text{subject to} \quad \sum_{i\in\mathcal{L}_k} \mu_i = 1, \tag{21b}$$

$$0 \le \mu_i \le 1, \ \forall i \in \mathcal{L}_k \tag{21c}$$

Note that for a one-tier super cell, (12) reduces to (10), as the $\min$ operator is associative. The generalized end-to-end sum rate for BS_i in the nth tier for $n = 1, 2, \ldots, N_{\mathrm{T}}$ becomes:

$$\mathcal{R}^{\mathrm{UBS}}_{\mathrm{BS}_i} = \sum_{u\in\mathcal{U}_i} \mathcal{R}^{\mathrm{UBS}}_u, \ \forall i \in \mathcal{T}_n \tag{13}$$

B. Cell-based Bandwidth Scheduling

The point that distinguishes CBS from UBS is that in CBS, the gateway puts up the entire data intended for each BS in an exclusive set of subcarriers of the bottleneck backhaul. Then, the desired BS assigns that given bandwidth equally to the associated UEs. The end-to-end sum rate of BS_i in the nth tier is expressed mathematically as follows:

$$\mathcal{R}^{\mathrm{CBS}}_{\mathrm{BS}_i} = \min\left[\min_{j\in\mathcal{P}_i} \mu_{i,j}\xi_{\mathrm{b}} B_{\mathrm{b}} \log_2(1+\gamma_{\mathrm{b}_j}), \frac{\xi_{\mathrm{a}} B_{\mathrm{a}}}{M_i}\sum_{u\in\mathcal{U}_i}\log_2(1+\gamma_u)\right], \ \forall i \in \mathcal{T}_n. \tag{14}$$

C. A System-Level Simplification

With the assumption that a fixed power P_{b} is equally assigned to every individual backhaul link, the received SNR of all the backhaul links become identical:

$$\gamma_{\mathrm{b}_i} = K_{\mathrm{b}}\gamma_{\mathrm{b}}, \ \forall i \in \mathcal{L}_k \tag{15}$$

where $K_{\mathrm{b}} = \frac{P_{\mathrm{b}}}{P_{\mathrm{a}}}$ is a common power control coefficient for the backhaul system[5]. A judicious design consists in choosing bandwidth allocation ratios for the outer tiers so that intermediate hops do not restrict the effective achievable rate in the path from the gateway to the desired BS. One such design is to make the bandwidth sharing coefficients in the outer tiers proportional to that of the bottleneck link according to the following normalization:

$$\mu_{i,j} = \frac{\mu_i}{\sum_{i'\in\mathcal{L}_j}\mu_{i'}} > \mu_i, \ \forall i \in \mathcal{L}_j \tag{16}$$

The inequality $\mu_{i,j} > \mu_i$ is derived from the fact that $\sum_{i'\in\mathcal{L}_j}\mu_{i'} < 1$ when $j \in \mathcal{T}_n \ \forall n > 1$. Thus:

$$\min_{j\in\mathcal{P}_i} \mu_{i,j} = \mu_i. \tag{17}$$

[5] K_{b} also represents the total power of the backhaul system normalized by that of the access system, i.e. $K_{\mathrm{b}} = \frac{\sum_{i\in\mathcal{L}_k} P_{\mathrm{b}_i}}{N_{\mathrm{BS}} P_{\mathrm{a}}}$.

1) UBS: By using (15) and (17), the term representing the rate of $\mathcal{P}_i$ in (12) simplifies to:

$$\min_{j\in\mathcal{P}_i} \mu_{i,j}\zeta\log_2(1+\gamma_{\mathrm{b}_j}) = \mu_i\zeta\log_2(1+\gamma_{\mathrm{b}_k}). \tag{18}$$

In effect, the dominant hop along the backhaul path is merely posed by the bottleneck link, i.e. b_k. For BS_i in the nth tier for $n = 1, 2, \ldots, N_{\mathrm{T}}$, the end-to-end transmission rate of the uth UE in (12) reduces to a more tractable form of:

$$\mathcal{R}^{\mathrm{UBS}}_u = \frac{\xi_{\mathrm{a}} B_{\mathrm{a}}}{M_i} \min\left[\mu_i\zeta\log_2(1+\gamma_{\mathrm{b}_k}), \log_2(1+\gamma_u)\right], \ \forall u \in \mathcal{U}_i \tag{19}$$

2) CBS: Based on (15) and (17), the end-to-end sum rate of BS_i in (14) is simplified to:

$$\mathcal{R}^{\mathrm{CBS}}_{\mathrm{BS}_i} = \min\left[\mu_i\xi_{\mathrm{b}} B_{\mathrm{b}}\log_2(1+\gamma_{\mathrm{b}_k}), \frac{\xi_{\mathrm{a}} B_{\mathrm{a}}}{M_i}\sum_{u\in\mathcal{U}_i}\log_2(1+\gamma_u)\right], \ \forall i \in \mathcal{T}_n. \tag{20}$$

In the following, the problems of bandwidth scheduling and power control are separately studied because the wireless optical backhaul system is assumed to be operating over a frequency-flat channel in which there is no gain in performing an adaptive power allocation among different subcarriers, as they all experience the same channel gain. In this case, the received power level is fixed on the entire bandwidth, and then the question is how to judiciously select the transmission power level for the backhaul system as a whole. With a fixed amount of power, a limited bandwidth may cause the backhaul system to run out of capacity, hence the available bandwidth needs to be optimally utilized, which is where optimal bandwidth scheduling comes into play.

IV. Optimal Bandwidth Scheduling

This section focuses on the problem of optimal bandwidth scheduling. In particular, the design of bandwidth sharing coefficients for the generalized case of multi-tier super cells is formulated as an optimization problem aiming for the end-to-end sum rate maximization.

A. Optimal User-based Bandwidth Scheduling

The purpose of optimal UBS is to maximize the sum of *per-user* end-to-end rates under the UBS policy. Based on (19), the optimization problem for the kth branch of the super cell is stated in the global form in (21), shown at the top of this page. The constraints (21b) and (21c) are declared in Section II-D. For global optimization of the bandwidth

$$\underset{\{\mu_i \in \mathbb{R}\}}{\text{maximize}} \quad \sum_{i\in\mathcal{L}_k} \min\left[\mu_i \xi_{\mathrm{b}} B_{\mathrm{b}} \log_2(1+\gamma_{\mathrm{b}_k}), \frac{\xi_{\mathrm{a}} B_{\mathrm{a}}}{M_i} \sum_{u\in\mathcal{U}_i} \log_2(1+\gamma_u)\right] \tag{26a}$$

$$\text{subject to} \quad \sum_{i\in\mathcal{L}_k} \mu_i = 1, \tag{26b}$$

$$0 \le \mu_i \le 1, \ \forall i \in \mathcal{L}_k \tag{26c}$$

allocation, the downlink SINR for entire UEs in the kth branch is processed by a central controller, provided that each BS collects the SINR information from an uplink channel and sends it to the central controller.

The objective function in (21a) can be expanded through dividing both arguments of the $\min$ operator by a constant term $\zeta \log_2(1+\gamma_{\mathrm{b}_k})$ and defining a variable ρ_u to be the normalized achievable rate for the uth UE:

$$\rho_u = \frac{\log_2(1+\gamma_u)}{\zeta \log_2(1+\gamma_{\mathrm{b}_k})}. \tag{22}$$

The factor $\xi_{\mathrm{b}} B_{\mathrm{b}} \log_2(1+\gamma_{\mathrm{b}_k})$ is independent of optimization variables and it can be put aside without affecting the problem in (21). This leads to a compact form of:

$$\underset{\{\mu_i \in \mathbb{R}\}}{\text{maximize}} \quad \sum_{i\in\mathcal{L}_k} \sum_{u\in\mathcal{U}_i} \frac{1}{M_i} \min[\mu_i, \rho_u] \tag{23a}$$

$$\text{subject to} \quad \text{(21b) \& (21c)} \tag{23b}$$

The objective function in (23a) is a composite of concave operators, comprising summation and minimization. Such a composition preserves concavity and the objective function is concave [25]. Therefore, this is a convex optimization problem with linear constraints, for which Slater's condition holds and there is a global optimum [26]. However, standard methods such as Lagrange multipliers cannot be directly applied to find an analytical solution because the objective function is not differentiable in $\boldsymbol{\mu} = [\mu_i]_{N_{\mathrm{BS}}\times 1}$, where $\boldsymbol{\mu}$ is the vector of optimization variables.

For nonsmooth optimization, the subgradient method is a means to deal with nondifferentiable convex functions [27]. Particularly, the constrained optimization problem in (23) can be efficiently solved by using the *projected* subgradient method. Analogous to common subgradient methods, the vector $\boldsymbol{\mu}$ is sequentially updated using a subgradient of the objective function at $\boldsymbol{\mu}$. Compared with an ordinary subgradient method, there is an additional constraint $\mathbf{1}^T\boldsymbol{\mu} = 1$, with $\mathbf{1}$ denoting an all-ones vector of size $N_{\mathrm{BS}} \times 1$, which is required by (21b). To fulfil this constraint, at each iteration, the projected approach maps the components of $\boldsymbol{\mu}$ onto a unit space before proceeding with the next update, to bring them back to the feasible set. The convergence is attained upon setting a suitable step size for executing iterations [27]. To develop an efficient iterative algorithm, an appropriate subgradient vector is required to provide a descent direction for a local maximizer to approach the global maximum when updating. To this end, the problem statement needs to be properly modified. The users in the attocell of BS_i are split into two disjoint groups: those for whom $\mu_i > \rho_u$ and those for whom $\mu_i \le \rho_u$. The index sets for these two groups are denoted by $\hat{\mathcal{U}}_i$ and $\check{\mathcal{U}}_i$, respectively, implying $\hat{\mathcal{U}}_i \cup \check{\mathcal{U}}_i = \mathcal{U}_i$. The number of elements corresponding to $\hat{\mathcal{U}}_i$ and $\check{\mathcal{U}}_i$ is represented by $\hat{M}_i$ and $\check{M}_i$ so that $\hat{M}_i + \check{M}_i = M_i$. The optimization problem in (23) is then stated in the desired form:

$$\underset{\{\mu_i \in \mathbb{R}\}}{\text{maximize}} \quad \sum_{i\in\mathcal{L}_k} \left[\sum_{u\in\hat{\mathcal{U}}_i} \frac{\rho_u}{M_i} + \frac{\check{M}_i}{M_i}\mu_i\right] \tag{24a}$$

$$\text{subject to} \quad \text{(21b) \& (21c)} \tag{24b}$$

Note that the arrangements of $\check{\mathcal{U}}_i$ and $\hat{\mathcal{U}}_i$ depend on the value of μ_i. Based on (24a), the derivative of the objective function with respect to μ_i is estimated by $\frac{\check{M}_i}{M_i}$, resulting in the subgradient vector $\mathbf{g} = [g_i]_{N_{\mathrm{BS}}\times 1}$ where $g_i = \frac{\check{M}_i}{M_i}$. The projected subgradient method for solving the primal problem is summarized in Algorithm 1. In the first line of this algorithm, α is the step size for updating, which is chosen to be sufficiently small; and in step 8, $\mathbf{P}$ is an $N_{\mathrm{BS}} \times N_{\mathrm{BS}}$ unitary space projection matrix [28], which is obtained as follows:

$$\mathbf{P} = \mathbf{I} - \mathbf{1}\left(\mathbf{1}^T\mathbf{1}\right)^{-1}\mathbf{1}^T = \mathbf{I} - \frac{1}{3}\mathbf{J}, \tag{25}$$

where $\mathbf{I}$ and $\mathbf{J}$ respectively represent an identity matrix and an all-ones matrix of size $N_{\mathrm{BS}} \times N_{\mathrm{BS}}$.

B. Optimal Cell-based Bandwidth Scheduling

The scheduler aims to maximize the aggregate *per-cell* end-to-end sum rates under the CBS policy by computing an optimal solution to the following bandwidth allocation problem. For the kth branch of the super cell, by using (20), the optimization problem is stated in (26), shown at the top of this page. The central controller only gathers the overall access sum rate information sent individually by each BS via the feedback channel for further processing. This reduces the feedback overhead with respect to UBS, which appeals to applications where limited feedback is available [29].

Similar to the optimal UBS case, the optimal CBS problem in (26) is reformulated as follows:

$$\underset{\{\mu_i \in \mathbb{R}\}}{\text{maximize}} \quad \sum_{i\in\mathcal{L}_k} \min\left[\mu_i, \frac{1}{M_i}\sum_{u\in\mathcal{U}_i} \rho_u\right] \tag{27a}$$

$$\text{subject to} \quad \text{(21b) \& (21c)} \tag{27b}$$

where ρ_u is given by (22). The projected subgradient method is used to solve the primal problem. With the current expression in (27a), the objective function is not differentiable in $\boldsymbol{\mu}$. To find the candidate subgradient vector, the BSs of the kth

Algorithm 1 Projected Subgradient Algorithm for Optimal User-based Bandwidth Scheduling.

Choose α
Initialize $\boldsymbol{\mu}^{(0)}$
for all $i \in \mathcal{L}_k$ **do**
  Let $\check{\mathcal{U}}_i^{(l)} = \left\{ u \in \mathcal{U}_i \middle| \mu_i^{(l)} \leq \rho_u \right\}$
  Compute $\check{M}_i^{(l)} = \left| \check{\mathcal{U}}_i^{(l)} \right|$
  Compute $g_i^{(l)} = \dfrac{\check{M}_i^{(l)}}{M_i}$
end for
Update $\boldsymbol{\mu}^{(l)}$ through $\boldsymbol{\mu}^{(l+1)} = \boldsymbol{\mu}^{(l)} - \alpha \mathbf{P}\mathbf{g}^{(l)}$
$l \leftarrow l + 1$
go to 3
Return $\boldsymbol{\mu}$

branch are classified into two categories: those that fulfil the condition $\mu_i > \frac{1}{M_i}\sum_{u\in\mathcal{U}_i}\rho_u$ and those that satisfy $\mu_i \leq \frac{1}{M_i}\sum_{u\in\mathcal{U}_i}\rho_u$. The former category is represented by an index set of $\hat{\mathcal{L}}_k$ and the latter case by $\check{\mathcal{L}}_k$. The optimization problem in (27) turns into:

$$\underset{\{\mu_i \in \mathbb{R}\}}{\text{maximize}} \quad \sum_{i\in\hat{\mathcal{L}}_k} \frac{1}{M_i} \sum_{u\in\mathcal{U}_i} \rho_u + \sum_{i\in\check{\mathcal{L}}_k} \mu_i \tag{28a}$$

$$\text{subject to} \quad \text{(21b) \& (21c)} \tag{28b}$$

Therefore, the derivative of the objective function with respect to μ_i is equal to 1, leading to the subgradient vector $\mathbf{g} = [g_i]_{N_{\mathrm{BS}}\times 1}$ where:

$$g_i = \begin{cases} 1, & i \in \check{\mathcal{L}}_k \\ 0, & i \in \hat{\mathcal{L}}_k \end{cases} \tag{29}$$

The projected subgradient method used to solve the primal problem is outlined in Algorithm 2.

C. Numerical Results and Discussions

This section presents performance results for optimal UBS and optimal CBS policies based on Algorithm 1 and Algorithm 2, respectively. To assess the optimality of the proposed algorithms, a baseline policy is required. To this end, a receiver-dependent bandwidth allocation strategy for tree topology is adopted from the domain of bandwidth sharing for multicast flows [30], by which the bandwidth of a shared link is apportioned among multiple, succeeding links proportionately with the number of receivers they serve. Inspired by such a strategy, proportionally weighted fair (PWF) bandwidth scheduling was devised [1]. The PWF scheduler allocates a fraction of bandwidth to each BS in proportion to the number of its associated UEs, i.e. $\mu_i = \frac{M_i}{M}\ \forall i \in \mathcal{L}_k$ for the kth branch of an N_{T}-tier super cell. The optimal scheduling case is marked with 'OPT' for distinction. The end-to-end sum rate performance is evaluated based on Section III. The achievable rate of the access network with an unlimited backhaul capacity is considered and labeled as 'Access Limit'. Monte-Carlo simulations are conducted over a large number of random realizations to distribute multiple UEs uniformly over the network. For a fair comparison between super cells with a different number of tiers, the results are presented in terms of the average UE density, which is defined as the ratio of the total number of UEs to that of BSs:

$$\lambda = \frac{M}{N_{\mathrm{BS}}} \text{ UE/Cell.} \tag{30}$$

Algorithm 2 Projected Subgradient Algorithm for Optimal Cell-based Bandwidth Scheduling.

Choose α
Initialize $\boldsymbol{\mu}^{(0)}$
Let $\check{\mathcal{L}}_k^{(l)} = \left\{ i \in \mathcal{L}_k \middle| \mu_i^{(l)} \leq \frac{1}{M_i}\sum_{u\in\mathcal{U}_i}\rho_u \right\}$
for all $i \in \mathcal{L}_k$ **do**
  if $i \in \check{\mathcal{L}}_k$ **then**
    Set $g_i^{(l)} = 1$
  else
    Set $g_i^{(l)} = 0$
  end if
end for
Update $\boldsymbol{\mu}^{(l)}$ through $\boldsymbol{\mu}^{(l+1)} = \boldsymbol{\mu}^{(l)} - \alpha \mathbf{P}\mathbf{g}^{(l)}$
$l \leftarrow l + 1$
go to 3
Return $\boldsymbol{\mu}$

The system parameters used for simulations are given as follows: downlink LED optical power, $P_{\mathrm{opt}} = 10$ W; downlink LED semi-angle, $\Phi_{\mathrm{a}} = 60°$; vertical separation, $h = 2.25$ m; hexagonal cell radius, $R = 3.1$ m; total VLC bandwidth, $B = 20$ MHz; IFFT/FFT length, $N = 1024$; noise power spectral density, $N_0 = 10^{-21}$ A^2/Hz; UE receiver field of view (FOV), $\Psi_{\mathrm{a}} = 85°$; PD effective area, $A_{\mathrm{PD}} = 10^{-4}$ m^2; PD responsivity, $R_{\mathrm{PD}} = 0.6$ A/W; and DC bias scaling factor, $\alpha = 3$. Configurations for cell radius and downlink LED semi-angle are adopted from the guidelines provided in [21]. Also: backhaul LED semi-angle, $\Phi_{\mathrm{b}} = 5°$, which is small enough to avoid crosstalk within backhaul links [19]; backhaul receiver FOV, $\Psi_{\mathrm{b}} = 85°$; and the backhaul link distance is equal to $\sqrt{3}R$.

Fig. 2 shows the average sum rate performance for one branch of an N_{T}-tier super cell as a function of the backhaul power ratio K_{b} for different values of N_{T} and λ. A key principle for understanding the impact of backhaul and access networks on the end-to-end performance relates to *rate limit*. This concept indicates the effective upper bound of the end-to-end sum rate imposed by both backhaul and access systems, i.e. $\min[\text{Backhaul Limit}, \text{Access Limit}]$[6]. For a low UE density scenario as shown in Fig. 2a, for $N_{\mathrm{T}} = 5$, both optimal policies maximally achieve the end-to-end rate limit over a broad range of values for K_{b}. Note that the optimal algorithms operate whether backhaul or access limits the end-to-end performance. Fig. 2a demonstrates when the difference between backhaul and access limits is large enough, both UBS-OPT and CBS-OPT fully attain the rate limit, which is the case for $K_{\mathrm{b}} < 10^{-3}$ and $K_{\mathrm{b}} \geq 10^{-1}$. Moreover, it can be observed that both UBS-OPT and CBS-OPT cases improve

[6]Backhaul Limit is defined as the achievable rate of the backhaul system per link.

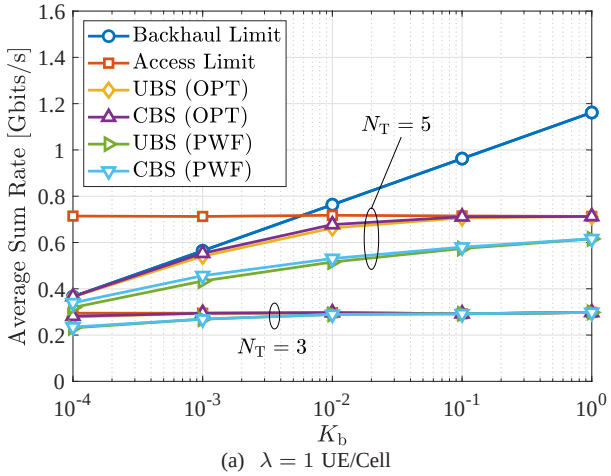

(a) $\lambda = 1$ UE/Cell

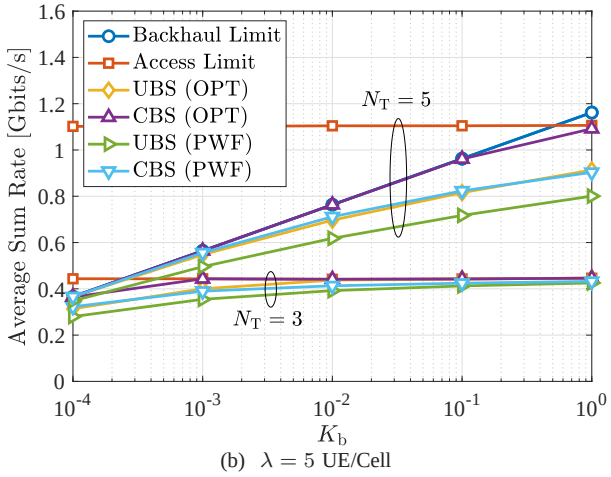

(b) $\lambda = 5$ UE/Cell

Fig. 2: Average sum rate performance of optimal UBS and optimal CBS policies as a the power ratio K_b for different values of N_T and λ; and $B_b = 3B_a$.

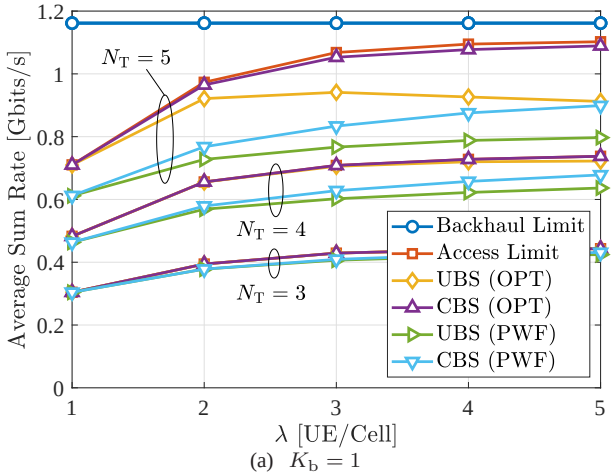

(a) $K_b = 1$

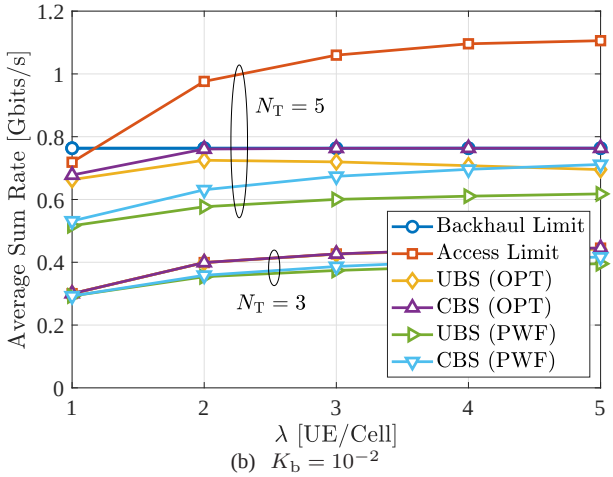

(b) $K_b = 10^{-2}$

Fig. 3: Average sum rate performance of optimal UBS and optimal CBS policies as a function of the UE density λ for different values of N_T and K_b; and $B_b = 3B_a$.

the performance against their respective baseline policies of UBS-PWF and CBS-PWF. The improvement is as much as 200 Mbits/s by choosing $K_b = 10^{-2}$. For $N_T = 3$, the overall rate of backhaul is sufficiently higher than that of access especially for $K_b \geq 10^{-2}$, in which case the performance for all scheduling policies coincide.

Fig. 2b plots the same set of results as in Fig. 2a, by considering a high UE density scenario of $\lambda = 5$ UE/Cell. Foremost, such an increase in the UE density causes the access rate limit to rise, which is more pronounced for $N_T = 5$. In this case, the backhaul enforces a bottleneck on the end-to-end transmission, and evidently CBS-OPT makes perfect use of the limited backhaul capacity by following its growing trend when K_b increases. For instance, CBS-OPT successfully reaches an average sum rate of just below 1 Gbits/s for $K_b = 10^{-1}$, as supplied by the backhaul system. Compared to Fig. 2a, the extent of improvement offered by optimal scheduling relative to PWF is lower in Fig. 2b, still this is enhanced by heightening the backhaul power. Furthermore, it is observed that CBS performs even better than UBS. There is also a small gap between the results of CBS and UBS in Fig. 2a, but the difference in performance is manifested in Fig. 2b when the number of UEs per cell is multiplied fivefold.

Fig.3 illustrates the average sum rate performance with respect to the UE density λ for different combinations of N_T and K_b. For $N_T = 5$, Fig.3a ($K_b = 1$) represents a case where the access limit is located under the backhaul limit, while Fig.3b ($K_b = 10^{-2}$) constitutes the converse case in which the backhaul limit dominates for the majority of values of λ. In either case, similar to Fig. 2, the optimal algorithms outperform their baseline counterparts. It is observed that CBS-OPT consistently retains the achievable rate limit as the UE density is increased. Also, CBS-OPT performs better than UBS-OPT, like the case in Fig. 2b. An explanation for this effect can be given by noting the operation principals of CBS and UBS systems. The per cell bandwidth allocation in CBS is compatible with the notion of the rate limit, which means it can efficiently adapt to the limits of access and backhaul networks. By contrast, the UBS system assigns the backhaul bandwidth in a per user basis and therefore introduces a degree of loss into the sum rate performance when aggregating the end-to-end rates achieved by individual UEs.

For completeness, the average sum rate performance versus the number of tiers N_{T} is presented in Fig. 4a; for $K_{\mathrm{b}} = 10^{-2}$ and $\lambda = 1$ UE/Cell. The effect of changing the backhaul bandwidth is also studied. For both cases of $B_{\mathrm{b}} = B_{\mathrm{a}}$ and $B_{\mathrm{b}} = 3B_{\mathrm{a}}$, by increasing N_{T}, performance gains of UBS-OPT and CBS-OPT with respect to UBS-PWF and CBS-PWF grow. In the case of $B_{\mathrm{b}} = B_{\mathrm{a}}$, backhaul is the main bottleneck of the end-to-end performance when deploying super cells with $N_{\mathrm{T}} \geq 3$. In this case, both optimal algorithms fully exploit the limited capacity of the bottleneck backhaul link as Fig. 4a shows. Increasing the bandwidth to $B_{\mathrm{b}} = 3B_{\mathrm{a}}$ provides adequate backhaul capacity and thus the access system becomes the major bottleneck. Again, the optimal UBS and optimal CBS exhibit a superior performance by achieving the maximum rate limit of the network. Note that expanding the size of super cells increases the chance for the backhaul system to turn into bottleneck for the end-to-end performance. In this case, the optimal bandwidth scheduling polices can make most use of the limited backhaul resources and hence they are *backhaul resource efficient*. For the same set of parameters as used in Fig. 4a, the average sum rate is plotted in Fig. 4b against the backhaul bandwidth normalized by the bandwidth of the access system, $\frac{B_{\mathrm{b}}}{B_{\mathrm{a}}}$.

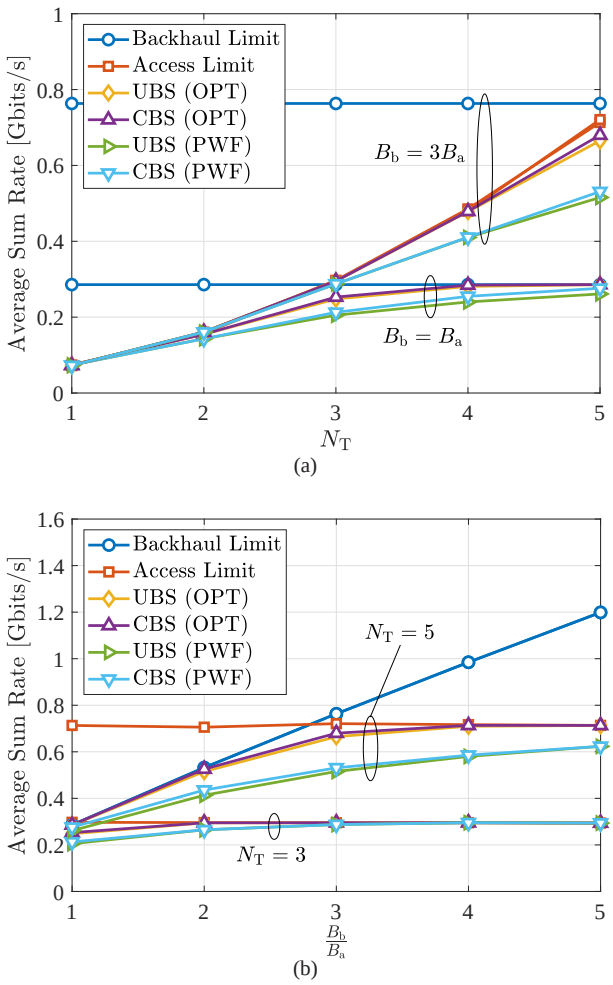

Fig. 4: Average sum rate performance of optimal UBS and optimal CBS policies for $K_{\mathrm{b}} = 10^{-2}$ and $\lambda = 1$ UE/Cell: (a) versus the total number of tiers N_{T}; (b) versus the bandwidth ratio $\frac{B_{\mathrm{b}}}{B_{\mathrm{a}}}$.

V. Opportunistic Power Control

The optical power of backhaul LEDs is opportunistically reduced with an incentive to enhance the PE of the backhaul system while maintaining the sum rate performance. A FPC strategy is proposed, whereby the transmission power in each backhaul branch is set to a constant operating point. This is a onetime design strategy, meaning that once an operating point is chosen, it remains the same for the entire backhaul branch. This greatly simplifies the implementation complexity when applying FPC to multi-tier super cells. However, an improperly low value of power can lead to a significant degradation in the network sum rate because of its impact on the capacity of the backhaul system. To reach a practical means to fix the backhaul power, three main schemes are put forward: MSPC, ASPC and ARPC. The performance of a given branch of the super cell depends on the overall rate of the corresponding bottleneck backhaul link. To prevent a backhaul bottleneck for the kth branch $\forall k \in \mathcal{T}_1$, the following condition needs to be satisfied:

$$\mathcal{R}_{\mathrm{b}_k} \geq \sum_{i \in \mathcal{L}_k} \mathcal{R}_{\mathrm{a}_i}. \tag{31}$$

The following analysis focuses on the design of the backhaul power control coefficient K_{b} based on the rate requirement of the bottleneck link[7]. The minimum value of K_{b} is denoted by $K_{\mathrm{b,min}}$.

A. Proposed Schemes

1) MSPC: The first criterion is to adjust the backhaul power in response to the maximum sum rate of the access system. The bounds of the access sum rate are related to those of the access SINR by noting that $\mathcal{R}_{\mathrm{a}_i}$ is a bounded random variable such that:

$$\mathcal{R}_{\min} \leq \mathcal{R}_{\mathrm{a}_i} \leq \mathcal{R}_{\max}, \tag{32}$$

where $\mathcal{R}_{\min} = \xi_{\mathrm{a}} B_{\mathrm{a}} \log_2(1 + \gamma_{\min})$ and $\mathcal{R}_{\max} = \xi_{\mathrm{a}} B_{\mathrm{a}} \log_2(1 + \gamma_{\max})$ in which $\gamma_{\min}$ and $\gamma_{\max}$ are available in (6). The associated MSPC ratio is derived in Proposition 1.

Proposition 1. *The minimum power control coefficient for b_k based on MSPC is given by:*

$$K_{\mathrm{b,min}} = \frac{(1 + \gamma_{\max})^{\zeta^{-1} N_{\mathrm{BS}}} - 1}{\gamma_{\mathrm{b}}}. \tag{33}$$

Proof. On the right hand side (RHS) of (31), $\mathcal{R}_{\mathrm{a}_i}$ is replaced by its upper limit from (32):

$$\begin{aligned} \xi_{\mathrm{b}} B_{\mathrm{b}} \log_2(1 + K_{\mathrm{b}} \gamma_{\mathrm{b}}) &\geq \sum_{i \in \mathcal{L}_k} \mathcal{R}_{\max}, \\ &= N_{\mathrm{BS}} \xi_{\mathrm{a}} B_{\mathrm{a}} \log_2(1 + \gamma_{\max}). \end{aligned} \tag{34}$$

[7]For the kth branch of the backhaul network, a feasible set is defined by $\mathcal{R}_{\mathrm{b}_i} \geq \sum_{j \in \mathcal{L}_i} \mathcal{R}_{\mathrm{a}_j}$, through the system of N_{BS} inequalities for all BS_i $\forall i \in \mathcal{L}_k$. Fulfilling the rate requirement of the bottleneck link b_k by (31) automatically guarantees validating the remaining inequalities for the higher tiers.

$$I_1 = \int_{\gamma_{\min}}^{\gamma_{\max}} \left(1 - \mathbb{P}\left[\gamma_u \leq \gamma\right]\right) d\gamma = \frac{\gamma_{\max} - \gamma_{\min}}{2} + \frac{2}{\pi R_{\mathrm{e}}^2} \int_{\gamma_{\min}}^{\gamma_{\max}} \int_{0}^{R_{\mathrm{e}}} \arcsin^{\dagger}\left(\mathcal{Z}(r,\gamma)\right) r dr d\gamma. \tag{38}$$

$$I_2 = \frac{\xi_{\mathrm{a}} B_{\mathrm{a}}}{\ln 2} \int_{\gamma_{\min}}^{\gamma_{\max}} \left(1 - \mathbb{P}\left[\gamma_u \leq \gamma\right]\right) \frac{d\gamma}{1+\gamma} = \frac{\mathcal{R}_{\max} - \mathcal{R}_{\min}}{2} + \frac{2\xi_{\mathrm{a}} B_{\mathrm{a}}}{\pi R_{\mathrm{e}}^2 \ln 2} \int_{\gamma_{\min}}^{\gamma_{\max}} \int_{0}^{R_{\mathrm{e}}} \frac{\arcsin^{\dagger}\left(\mathcal{Z}(r,\gamma)\right) r}{1+\gamma} dr d\gamma. \tag{45}$$

Note that $|\mathcal{L}_k| = N_{\mathrm{BS}}\ \forall k \in \mathcal{T}_1$. Expressing the inequality in (34) in terms of K_{b} gives rise to:

$$K_{\mathrm{b}} \geq \frac{(1+\gamma_{\max})^{\zeta^{-1} N_{\mathrm{BS}}} - 1}{\gamma_{\mathrm{b}}}. \tag{35}$$

The minimum value of K_{b} is readily given by the RHS of (35), which is the desired result. ■

2) ASPC: The second criterion is to allocate power to the backhaul system so as to satisfy the achievable rate corresponding to the statistical average of the downlink SINR over the area covered by each attocell. The average SINR of the access system is given by Lemma 1. The ASPC ratio is then derived in Proposition 2.

Lemma 1. *The average downlink SINR is calculated by:*

$$\bar{\gamma}_{\mathrm{a}} = \frac{\gamma_{\min} + \gamma_{\max}}{2} + \frac{2}{\pi R_{\mathrm{e}}^2} \int_{\gamma_{\min}}^{\gamma_{\max}} \int_{0}^{R_{\mathrm{e}}} \arcsin^{\dagger}\left(\mathcal{Z}(r,\gamma)\right) r dr d\gamma. \tag{36}$$

Proof. Note that different UEs have the same average rate since $\gamma_u\ \forall u$ are independent and identically distributed (i.i.d.). The expected value of a bounded random variable X such that $x_{\min} \leq X \leq x_{\max}$ is $\mathbb{E}[X] = x_{\min} + \int_{x_{\min}}^{x_{\max}} \mathbb{P}[X > x] dx$. The average downlink SINR is derived as:

$$\bar{\gamma}_{\mathrm{a}} = \gamma_{\min} + \underbrace{\int_{\gamma_{\min}}^{\gamma_{\max}} \mathbb{P}\left[\gamma_u > x\right] dx}_{I_1}. \tag{37}$$

By using the CDF of γ_u in (3), I_1 is evaluated as in (38), shown at the top of this page. Substituting I_1 in (37) with (38) results in (36). ■

Proposition 2. *The minimum power control coefficient for b_k based on ASPC is given by:*

$$K_{\mathrm{b,min}} = \frac{(1+\bar{\gamma}_{\mathrm{a}})^{\zeta^{-1} N_{\mathrm{BS}}} - 1}{\gamma_{\mathrm{b}}}, \tag{39}$$

where $\bar{\gamma}_{\mathrm{a}}$ is the average downlink SINR given by Lemma 1.

Proof. In the case of ASPC, the inequality in (31) changes to:

$$\xi_{\mathrm{b}} B_{\mathrm{b}} \log_2(1 + K_{\mathrm{b}} \gamma_{\mathrm{b}}) \geq \sum_{i \in \mathcal{L}_k} \xi_{\mathrm{a}} B_{\mathrm{a}} \log_2(1 + \mathbb{E}[\gamma_u]), \tag{40}$$

where $\mathbb{E}[\gamma_u] = \bar{\gamma}_{\mathrm{a}}$. It immediately follows that:

$$K_{\mathrm{b}} \geq \frac{(1+\bar{\gamma}_{\mathrm{a}})^{\zeta^{-1} N_{\mathrm{BS}}} - 1}{\gamma_{\mathrm{b}}}. \tag{41}$$

The RHS of (41) is, in fact, the minimum value that K_{b} can take and this concludes the proof. ■

3) ARPC: The third criterion for assigning power to the backhaul system takes into account the statistical average of the achievable rate for the access system over the area covered by each attocell. The average data rate of the access system is provided in Lemma 2. The ARPC ratio is subsequently derived in Proposition 3.

Lemma 2. *The average achievable rate of the access system per attocell is calculated by:*

$$\bar{\mathcal{R}}_{\mathrm{a}} = \frac{\mathcal{R}_{\min} + \mathcal{R}_{\max}}{2} + \frac{2\xi_{\mathrm{a}} B_{\mathrm{a}}}{\pi R_{\mathrm{e}}^2 \ln 2} \int_{\gamma_{\min}}^{\gamma_{\max}} \int_{0}^{R_{\mathrm{e}}} \frac{\arcsin^{\dagger}\left(\mathcal{Z}(r,\gamma)\right) r}{1+\gamma} dr d\gamma. \tag{42}$$

Proof. By using (8a), the average access system rate for BS$_i$ is obtained as:

$$\mathbb{E}\left[\mathcal{R}_{\mathrm{a}_i}\right] = \xi_{\mathrm{a}} B_{\mathrm{a}}\, \mathbb{E}\left[\log_2(1+\gamma_u)\right]. \tag{43}$$

Note that $\gamma_u\ \forall u \in \mathcal{U}_i$ are i.i.d., thus $\mathbb{E}\left[\mathcal{R}_{\mathrm{a}_i}\right] = \bar{\mathcal{R}}_{\mathrm{a}}\ \forall i$. Based on (3), the expectation in (43) is therefore expanded as follows:

$$\bar{\mathcal{R}}_{\mathrm{a}} = \mathcal{R}_{\min} + \underbrace{\int_{\mathcal{R}_{\min}}^{\mathcal{R}_{\max}} \mathbb{P}\left[\xi_{\mathrm{a}} B_{\mathrm{a}} \log_2(1+\gamma_u) > x\right] dx}_{I_2}, \tag{44}$$

where I_2 is derived in (45), shown at the top of this page. The substitution $x = \xi_{\mathrm{a}} B_{\mathrm{a}} \log_2(1+\gamma)$ is used to arrive at (45), which does not alter the inequality under a probability measure as the logarithm is a monotonically increasing function. Replacing I_2 in (44) by (45) and simplifying leads to (42). ■

Proposition 3. *The minimum power control coefficient for b_k based on ARPC is given by:*

$$K_{\mathrm{b,min}} = \frac{\exp\left(\frac{\ln 2}{\xi_{\mathrm{b}} B_{\mathrm{b}}} N_{\mathrm{BS}} \bar{\mathcal{R}}_{\mathrm{a}}\right) - 1}{\gamma_{\mathrm{b}}}, \tag{46}$$

where $\bar{\mathcal{R}}_{\mathrm{a}}$ is the average achievable rate over an attocell, given by Lemma 2.

Proof. According to ARPC, the RHS of (31) needs to be modified as follows:

$$\xi_{\mathrm{b}} B_{\mathrm{b}} \log_2(1 + K_{\mathrm{b}} \gamma_{\mathrm{b}}) \geq \mathbb{E}\left[\sum_{i \in \mathcal{L}_k} \mathcal{R}_{\mathrm{a}_i}\right] = N_{\mathrm{BS}} \bar{\mathcal{R}}_{\mathrm{a}}. \tag{47}$$

Rearranging the inequality in terms of K_{b} gives:

$$K_{\mathrm{b}} \geq \frac{\exp\left(\frac{\ln 2}{\xi_{\mathrm{b}} B_{\mathrm{b}}} N_{\mathrm{BS}} \bar{\mathcal{R}}_{\mathrm{a}}\right) - 1}{\gamma_{\mathrm{b}}}. \tag{48}$$

$$\mathbb{E}\left[\mathcal{R}_{\mathrm{a}}^2(\gamma_u)\right] = \frac{\mathcal{R}_{\min}^2 + \mathcal{R}_{\max}^2}{2} + \frac{1}{\pi}\left(\frac{2\xi_{\mathrm{a}}B_{\mathrm{a}}}{R_{\mathrm{e}}\ln 2}\right)^2 \int_{\gamma_{\min}}^{\gamma_{\max}} \int_{0}^{R_{\mathrm{e}}} \frac{\ln(1+\gamma)}{1+\gamma} \arcsin^{\dagger}\left(\mathcal{Z}(r,\gamma)\right) r dr d\gamma. \tag{51}$$

$$I_3 = 2\left(\frac{\xi_{\mathrm{a}}B_{\mathrm{a}}}{\ln 2}\right)^2 \int_{\gamma_{\min}}^{\gamma_{\min}} \frac{\ln(1+\gamma)}{1+\gamma}\left(1-\mathbb{P}\left[\gamma_u \le \gamma\right]\right) d\gamma = \frac{\mathcal{R}_{\max}^2 - \mathcal{R}_{\min}^2}{2} + \frac{1}{\pi}\left(\frac{2\xi_{\mathrm{a}}B_{\mathrm{a}}}{R_{\mathrm{e}}\ln 2}\right)^2 \int_{\gamma_{\min}}^{\gamma_{\max}} \int_{0}^{R_{\mathrm{e}}} \frac{\ln(1+\gamma)}{1+\gamma} \arcsin^{\dagger}\left(\mathcal{Z}(r,\gamma)\right) r dr d\gamma. \tag{53}$$

The RHS of (48) represents the minimum allowed value of K_{b} and hence the proof is complete. ■

B. Probability of Backhaul Bottleneck Occurrence

To gain insight into the power control performance, a metric called BBO is defined as follows.

Definition 1. *BBO is a metric to measure the probability that the aggregate sum rate of the access system in a backhaul branch exceeds the capacity of the corresponding bottleneck link. Equivalently, it evaluates the probability that the condition in* (31) *is violated.*

Mathematically, the BBO probability for the kth branch $k \in \mathcal{T}_1$, is expressed by:

$$P_{\mathrm{BBO}} = \mathbb{P}\left[\sum_{i\in\mathcal{L}_k} \mathcal{R}_{\mathrm{a}_i} > \mathcal{R}_{\mathrm{b}_k}\right], \tag{49}$$

where $\mathcal{R}_{\mathrm{a}_i}$ is a random variable that depends on the statistics of γ_u. There is no exact closed form solution for (49) in terms of ordinary functions. Alternatively, a simple but tight analytical approximation is established in Theorem 1 with the aid of Lemma 4. Note that $\mathcal{R}_{\mathrm{a}_i} = \frac{1}{M_i}\sum_{u\in\mathcal{U}_i}\mathcal{R}_{\mathrm{a}}(\gamma_u)$ where $\mathcal{R}_{\mathrm{a}}(\gamma_u) = \xi_{\mathrm{a}}B_{\mathrm{a}}\log_2(1+\gamma_u)$ are i.i.d.. The mean of $\mathcal{R}_{\mathrm{a}}(\gamma_u)$ is readily given by Lemma 2. The variance of $\mathcal{R}_{\mathrm{a}}(\gamma_u)$ is determined in Lemma 3.

Lemma 3. *The variance of $\mathcal{R}_{\mathrm{a}}(\gamma_u)$ is:*

$$\sigma_{\mathcal{R}_{\mathrm{a}}}^2 = \mathbb{E}\left[\mathcal{R}_{\mathrm{a}}^2(\gamma_u)\right] - \mathbb{E}^2[\mathcal{R}_{\mathrm{a}}(\gamma_u)], \tag{50}$$

where $\mathbb{E}\left[\mathcal{R}_{\mathrm{a}}(\gamma_u)\right] = \bar{\mathcal{R}}_{\mathrm{a}}$ and $\mathbb{E}[\mathcal{R}_{\mathrm{a}}^2(\gamma_u)]$ is given by (51)*, shown at the top of this page.*

Proof. The second order moment of a bounded random variable $x_{\min} \le X \le x_{\max}$ is characterized by using $\mathbb{E}\left[X^2\right] = x_{\min}^2 + \int_{x_{\min}}^{x_{\max}} 2x\mathbb{P}[X > x]dx$. Therefore:

$$\mathbb{E}\left[\mathcal{R}_{\mathrm{a}}^2(\gamma_u)\right] = \mathcal{R}_{\min}^2 + \underbrace{\int_{\mathcal{R}_{\min}}^{\mathcal{R}_{\max}} 2x\mathbb{P}\left[\mathcal{R}_{\mathrm{a}}(\gamma_u) > x\right] dx}_{I_3}. \tag{52}$$

Referring to the CDF of γ_u in (3), I_3 is derived as in (53), shown at the top of this page. By substituting (53) for I_3 in (52), the desired result of (51) is deduced. ■

Theorem 1. *For the kth backhaul branch with M UEs over the total area covered by N_{BS} BSs, the BBO probability is tightly approximated by:*

$$P_{\mathrm{BBO}} \approx \sum_{n=1}^{N_{\mathrm{BS}}} p_n \mathrm{Q}\left(\frac{\mathcal{R}_{\mathrm{b}_k} - n\bar{\mathcal{R}}_{\mathrm{a}}}{\frac{n}{\sqrt{M}}\sigma_{\mathcal{R}_{\mathrm{a}}}}\right), \tag{54}$$

where:

$$p_n = \binom{N_{\mathrm{BS}}}{n}\sum_{l=0}^{n}(-1)^l\binom{n}{l}\left(\frac{n-l}{N_{\mathrm{BS}}}\right)^M. \tag{55}$$

Also, $\mathcal{R}_{\mathrm{b}_k}$ and $\bar{\mathcal{R}}_{\mathrm{a}}$ are given by (8b) *and Lemma 2, respectively; and $\sigma_{\mathcal{R}_{\mathrm{a}}}$ is the standard deviation of $\mathcal{R}_{\mathrm{a}}(\gamma_u)$ whose variance is identified in Lemma 3.*

Proof. Let the vector $\mathbf{M} = [M_i]_{N_{\mathrm{BS}}\times 1}$ be composed of the random numbers of UEs in individual attocells for the kth branch. Provided that the total number of UEs is fixed at $\sum_{i\in\mathcal{L}_k} M_i = M$, $\mathbf{M}$ follows a multinomial distribution. The BBO probability in (49) is expressed as follows:

$$P_{\mathrm{BBO}} = \mathbb{P}\left[\sum_{i\in\mathcal{L}_k}\frac{1}{M_i}\sum_{u\in\mathcal{U}_i}\mathcal{R}_{\mathrm{a}}(\gamma_u) > \mathcal{R}_{\mathrm{b}_k}\right]. \tag{56}$$

The argument of the probability in (56) involves positive weights encompassing the reciprocals of the numbers of UEs in every attocell. An appropriate approximation of this weighted sum can be derived by means of minimizing the mean square error (MSE). This is presented in Lemma 4.

Lemma 4. *Based on the minimum mean square error (MMSE) criterion, the summation under the probability in* (56) *is approximated as follows:*

$$\sum_{i\in\mathcal{L}_k}\frac{1}{M_i}\sum_{u\in\mathcal{U}_i}\mathcal{R}_{\mathrm{a}}(\gamma_u) \approx \frac{n_{\mathrm{BS}}}{M}\sum_{i\in\mathcal{L}_k}\sum_{u\in\mathcal{U}_i}\mathcal{R}_{\mathrm{a}}(\gamma_u), \tag{57}$$

where n_{BS} indicates the aggregate number of non-empty attocells corresponding to the random vector $\mathbf{M}$. The attocell of BS$_i$ is accounted non-empty if $M_i > 0$.

Proof. Due to page limit, this proof is given in the preprint version [20]; see Appendix. ■

Let $Z = \frac{n_{\mathrm{BS}}}{M}\sum_{i\in\mathcal{L}_k}\sum_{u\in\mathcal{U}_i}\mathcal{R}_{\mathrm{a}}(\gamma_u)$. Note that Z is not directly dependent on the exact number of UEs that each attocell involves, i.e. the elements of $\mathbf{M}$. Rather, it depends on the overall number of non-empty attocells, i.e. n_{BS}. For each random experiment, n_{BS} takes integer values from 1 to N_{BS}. Besides, $\sum_{i\in\mathcal{L}_k}\sum_{u\in\mathcal{U}_i}\mathcal{R}_{\mathrm{a}}(\gamma_u)$ is a sum of M i.i.d. random

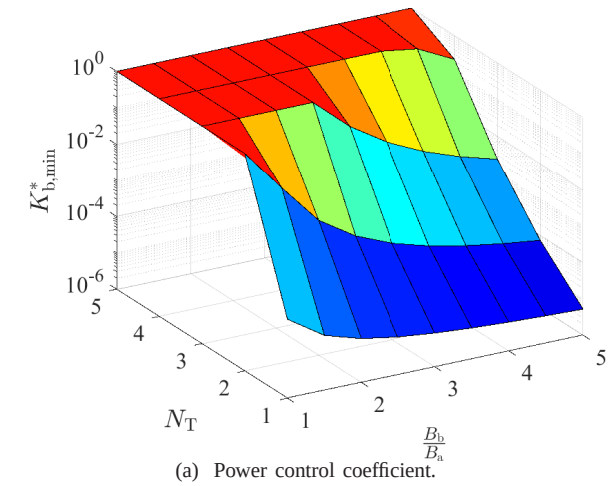

(a) Power control coefficient.

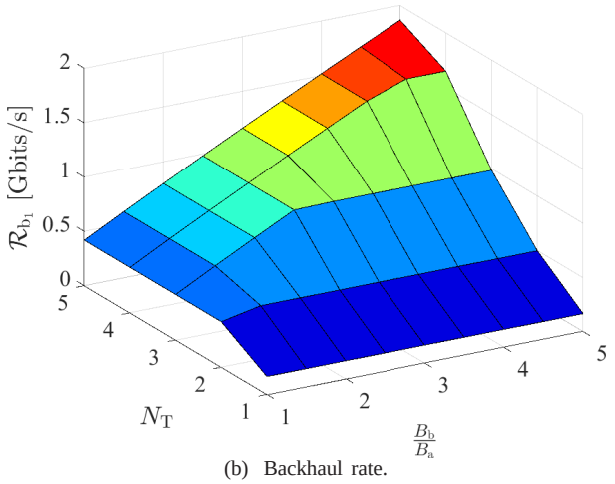

(b) Backhaul rate.

Fig. 5: $K^*_{\mathrm{b,min}}$ for MSPC and the backhaul rate $\mathcal{R}_{\mathrm{b}_1}|_{K_{\mathrm{b}}=K^*_{\mathrm{b,min}}}$ as a function of the total number of tiers N_{T} and the bandwidth ratio $\frac{B_{\mathrm{b}}}{B_{\mathrm{a}}}$.

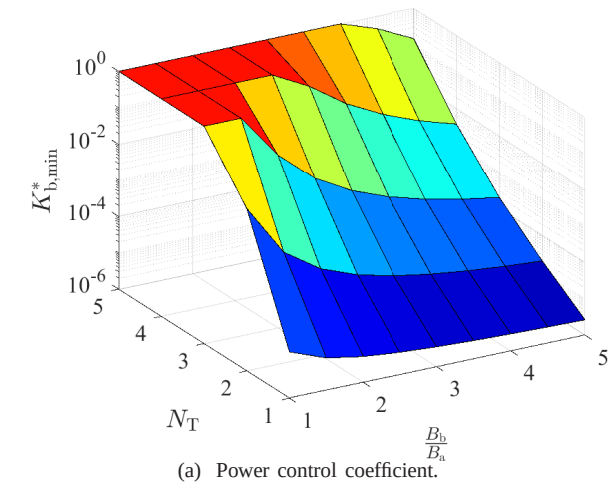

(a) Power control coefficient.

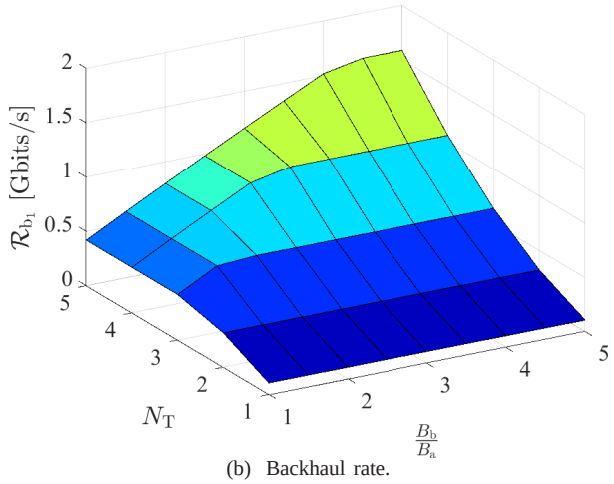

(b) Backhaul rate.

Fig. 6: $K^*_{\mathrm{b,min}}$ for ASPC and the backhaul rate $\mathcal{R}_{\mathrm{b}_1}|_{K_{\mathrm{b}}=K^*_{\mathrm{b,min}}}$ as a function of the total number of tiers N_{T} and the bandwidth ratio $\frac{B_{\mathrm{b}}}{B_{\mathrm{a}}}$.

variables $\mathcal{R}_{\mathrm{a}}(\gamma_u)$, the mean and variance of which are known according to Lemma 2 and Lemma 3, respectively. Thus, for a sufficiently large value of M, the conditional distribution of Z given $n_{\mathrm{BS}} = n$ converges to Gaussian based on the central limit theorem (CLT) [31]. It is deduced that:

$$Z\big|\{n_{\mathrm{BS}} = n\} \sim \mathcal{N}\left(n\bar{\mathcal{R}}_{\mathrm{a}}, \frac{n^2}{M}\sigma^2_{\mathcal{R}_{\mathrm{a}}}\right). \tag{58}$$

Therefore, by means of Lemma 4, the BBO probability in (56) can be evaluated by conditioning on n_{BS} and applying the law of total probability. Combining (58) with (57) and substituting the result into (56) gives rise to:

$$\begin{aligned} P_{\mathrm{BBO}} &\approx \sum_{n=1}^{N_{\mathrm{BS}}} \mathbb{P}\left[n_{\mathrm{BS}} = n\right] \mathbb{P}\left[Z > \mathcal{R}_{\mathrm{b}_k}\big|n_{\mathrm{BS}} = n\right], \\ &= \sum_{n=1}^{N_{\mathrm{BS}}} p_n \mathrm{Q}\left(\frac{\mathcal{R}_{\mathrm{b}_k} - n\bar{\mathcal{R}}_{\mathrm{a}}}{\frac{n}{\sqrt{M}}\sigma_{\mathcal{R}_{\mathrm{a}}}}\right), \end{aligned} \tag{59}$$

where $p_n = \mathbb{P}\left[n_{\mathrm{BS}} = n\right]$. From combinatorial analysis, the problem of distributing M UEs into N_{BS} attocells refers to the classical occupancy problem with Boltzmann-Maxwell statistics [32]. That is to say, there are N_{BS}^M permutations and each possible permutation has a probability of $\frac{1}{N_{\mathrm{BS}}^M}$[8]. Besides, the outcome of the event $\{n_{\mathrm{BS}} = n\}$ corresponds to the case where exactly n attocells each are occupied by at least one UE and the other $N_{\mathrm{BS}} - n$ remain empty. Let $\{n'_{\mathrm{BS}} = n'\}$ be the event indicating that exactly n' attocells are empty. The probability of this event is available in closed form [32]:

$$\begin{aligned} &\mathbb{P}\left[n'_{\mathrm{BS}} = n'\right] = \\ &\binom{N_{\mathrm{BS}}}{n'} \sum_{l=0}^{N_{\mathrm{BS}}-n'} (-1)^l \binom{N_{\mathrm{BS}} - n'}{l} \left(1 - \frac{n'+l}{N_{\mathrm{BS}}}\right)^M. \end{aligned} \tag{60}$$

Upon substituting $n' = N_{\mathrm{BS}} - n$, (60) reduces to the desired probability p_n in (55). ■

C. Numerical Results and Discussions

This section presents a number of case studies to evaluate the performance of the proposed power control schemes using computer simulations. The system parameters are the same as those listed in Section IV-C.

[8]This is an immediate result of the uniform distribution of UEs.

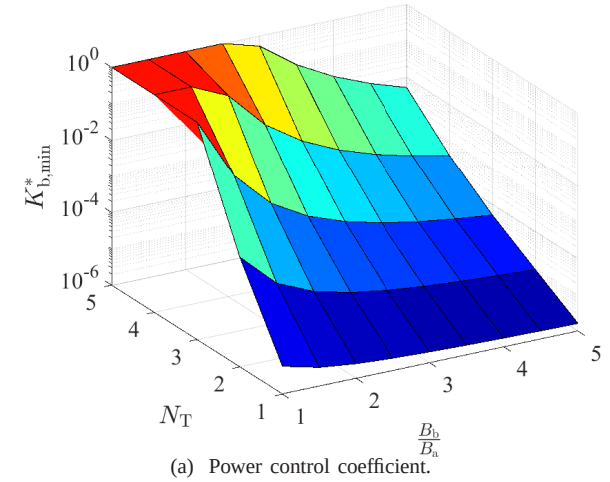

(a) Power control coefficient.

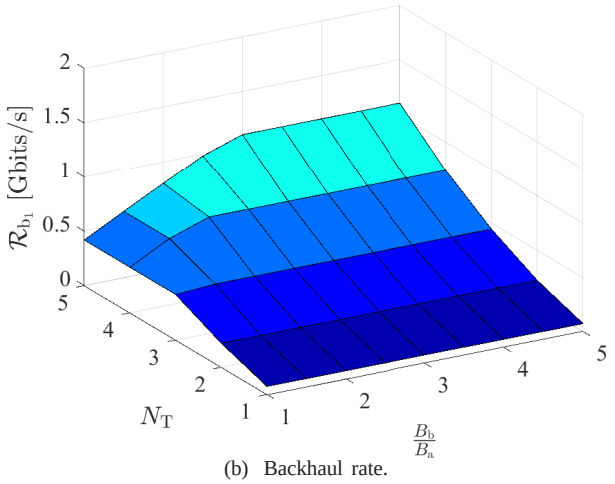

(b) Backhaul rate.

Fig. 7: $K^*_{\mathrm{b,min}}$ for ARPC and the backhaul rate $\mathcal{R}_{\mathrm{b}_1}|_{K_{\mathrm{b}}=K^*_{\mathrm{b,min}}}$ as a function of the total number of tiers N_{T} and the bandwidth ratio $\frac{B_{\mathrm{b}}}{B_{\mathrm{a}}}$.

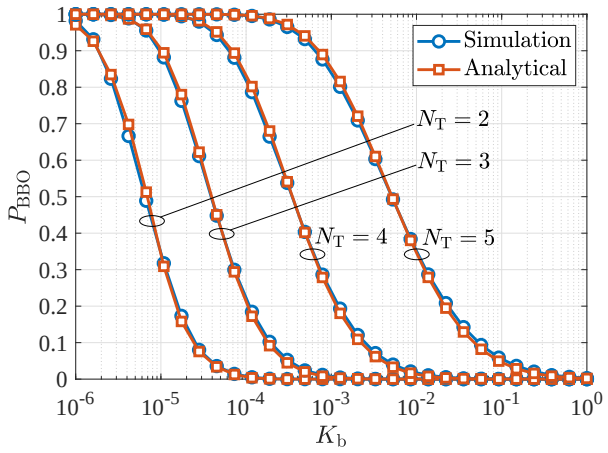

(a) $\lambda = 1$ UE/Cell

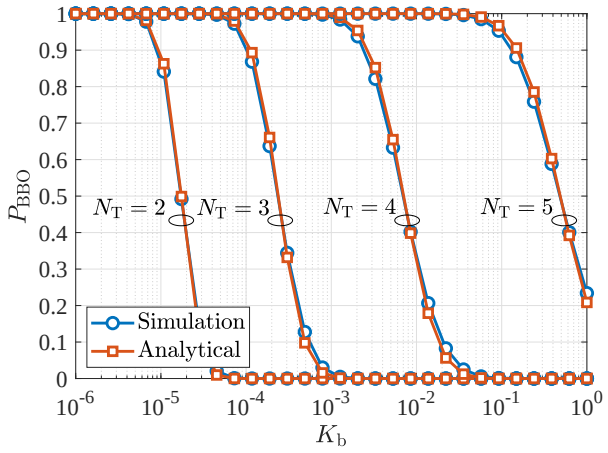

(b) $\lambda = 5$ UE/Cell

Fig. 8: Analytical and simulation results of the BBO probability as a function of K_{b} for different values of N_{T} and λ; and $B_{\mathrm{b}} = 3B_{\mathrm{a}}$. Analytical results are based on (54).

1) Power Control Coefficients: First, the range of variations of the power control coefficients is studied based on Propositions 1, 2 and 3 for MSPC, ASPC and ARPC, respectively.

Figs. 5a, 6a and 7a demonstrates the range of values of $K_{\mathrm{b,min}}$ for MSPC, ASPC and ARPC schemes, respectively, as a function of N_{T} and the bandwidth ratio $\frac{B_{\mathrm{b}}}{B_{\mathrm{a}}}$. The resulting backhaul rate for each scheme is computed by $\mathcal{R}_{\mathrm{b}_1}|_{K_{\mathrm{b}}=K^*_{\mathrm{b,min}}} = \xi_{\mathrm{b}} B_{\mathrm{b}} \log_2(1 + K^*_{\mathrm{b,min}}\gamma_{\mathrm{b}})$ and shown in Figs. 5b, 6b and 7b. It is observed that the power control coefficient is an increasing function of the total number of the deployed tiers for all three schemes, while it is a decreasing function of the normalized bandwidth. For given values of N_{T} and $\frac{B_{\mathrm{b}}}{B_{\mathrm{a}}}$, the highest value of $K_{\mathrm{b,min}}$ is set by MSPC, the second highest by ASPC, and the lowest by ARPC, confirming that:

$$K^{\mathrm{ARPC}}_{\mathrm{b,min}} < K^{\mathrm{ASPC}}_{\mathrm{b,min}} < K^{\mathrm{MSPC}}_{\mathrm{b,min}}. \tag{61}$$

The amount of power assigned to the backhaul system by the three schemes and the corresponding backhaul rates also obey the same rule in (61). For a fixed number of tiers, Figs. 5a, 6a and 7a show that by increasing the backhaul bandwidth, the level of $K_{\mathrm{b,min}}$ lessens for all the schemes altogether. Hence, more power needs to be allocated to the backhaul system when the bandwidth reduces. This conforms to the intrinsic power-bandwidth tradeoff governing the bottleneck link capacity to be shared between multiple downlink paths [19].

The power control coefficients rise continuously with increase in N_{T}, as observed from Fig. 5. However, they are not allowed to be increased unboundedly due to practical limitations imposed by the maximum permissible optical power of backhaul LEDs. To set an upper limit for the transmission power of the backhaul system, its counterpart from the access system, P_{a}, is used, as the access system operates with full power to comply with the illumination requirement[9]. This exerts a unit threshold constraint on $K_{\mathrm{b,min}}$, resulting in:

$$K^*_{\mathrm{b,min}} = \min[K_{\mathrm{b,min}}, 1]. \tag{62}$$

2) BBO Probability: For each branch of the super cell, the BBO probability can be analytically predicted by way of its

[9]The maximum allowable backhaul power could be an independent variable to model the practical specification of backhaul LEDs. Despite this possibility, setting a value equal to the power used in the access system simplifies the presentation of results, though it does not influence the generality of the power control analysis.

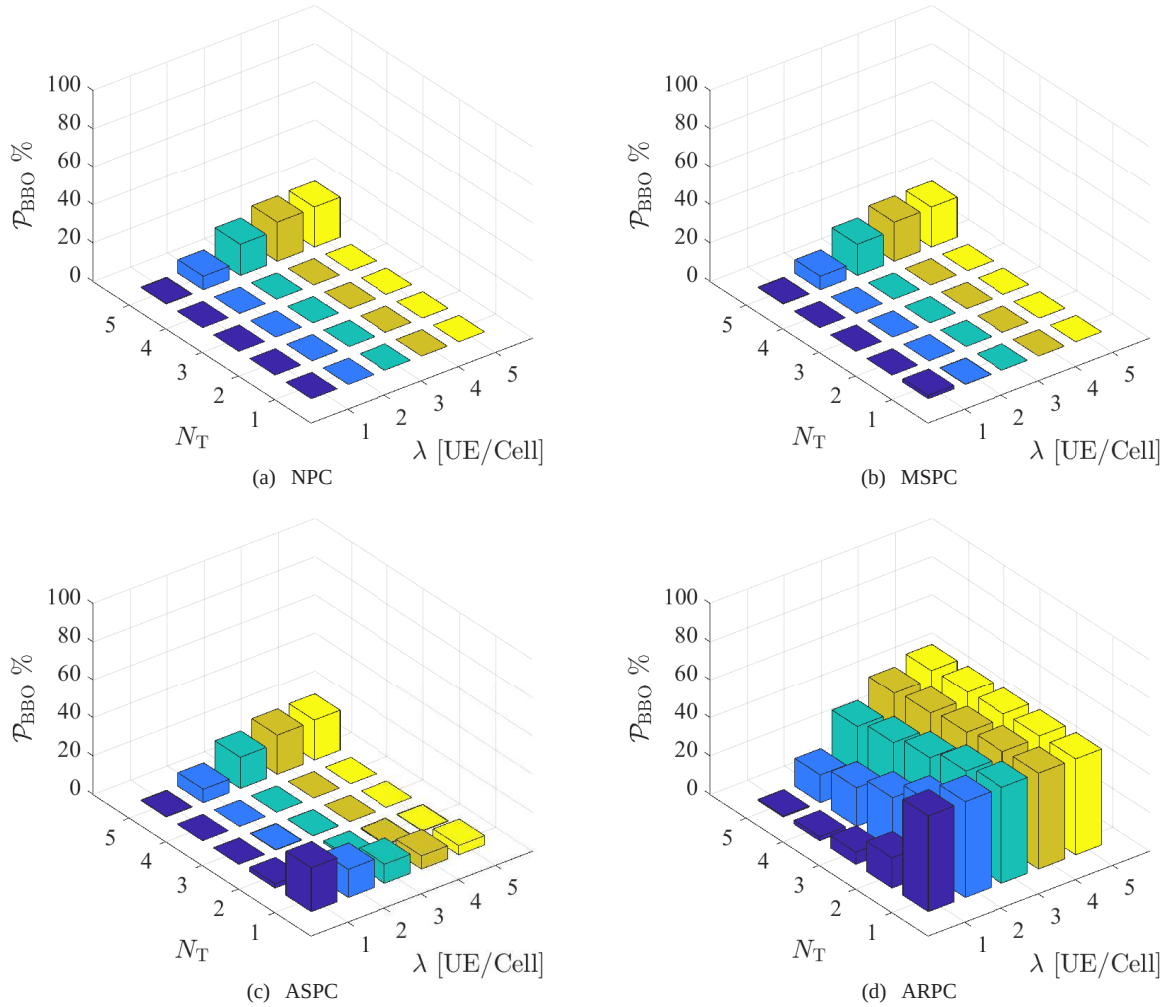

(a) NPC (b) MSPC

(c) ASPC (d) ARPC

Fig. 9: The BBO probability for NPC, MSPC, ASPC and ARPC schemes versus the total number of tiers N_{T} and the UE density λ for $B_{\mathrm{b}} = 3B_{\mathrm{a}}$.

approximate expression provided in Theorem 1. To verify the derivation of (54), the analytical and simulation results are plotted in Fig. 8 over a wide range of values of the power ratio K_{b}. Note that P_{BBO} is a function of K_{b} through $\mathcal{R}_{\mathrm{b}_1}$. The simulation results are directly obtained by computing the BBO probability in the Monte Carlo domain according to Definition 1. For comparison, different combinations of the total number of tiers, N_{T}, and the average UE density, λ, are considered.

For both cases of $\lambda = 1$ UE/Cell and $\lambda = 5$ UE/Cell, as shown in Figs. 8a and 8b, respectively, the analytical results closely match with those of the simulations. Nonetheless, there is a slight discrepancy between the two sets of results, because of the underlying approximation. Note that the analytical expression is neither an upper bound nor a lower bound of the BBO probability, as it is derived on the basis of the MMSE criterion. These results confirm that the formula derived in (54), though its simple form, does estimate well the actual BBO performance of super cells.

To shed light on another aspect of the backhaul power control, the resulting BBO probability of MSPC, ASPC and ARPC schemes are shown with a percent scale in Fig. 9 as a function of N_{T} and λ, for a fixed bandwidth of $B_{\mathrm{b}} = 3B_{\mathrm{a}}$. These results are obtained by using (54). The performance of a system with no power control (NPC) in which $P_{\mathrm{b}_i} = P_{\mathrm{a}}$ $\forall i$ is included for comparison. The results are consistent with those in Figs. 5, 6 and 7 in the sense that allocating higher power to the backhaul system leads to overall lower values of the BBO probability. It is observed that MSPC achieves almost equal BBO performance as the baseline NPC scheme. This is expected from the way MSPC is devised by using a high power value just enough to ensure that no backhaul bottleneck takes place, subject to the allowable limit. That is why for both NPC and MSPC, the BBO probability is zero for all cases of λ and $N_{\mathrm{T}} < 5$. For $N_{\mathrm{T}} = 5$, however, there is a nonzero chance that the required power to satisfy the access sum rate exceeds the allowed power threshold and therefore backhaul bottleneck inevitably occurs. In this case, the BBO probability is increased by adding more UEs, reaching 20% for $\lambda = 5$ UE/Cell.

Besides, ASPC performs similar to NPC and MSPC, except for $N_{\mathrm{T}} = 1$. This can be explained by noting that a one-tier

super cell involves one attocell per branch, thus any value of $\lambda \geq 1$ UE/Cell causes the only attocell of the branch to always be occupied. Unlike MSPC, the required power to avoid a backhaul bottleneck in response to such a load may be larger than what ASPC computes. The mentioned effect diminishes by increasing the UE density as shown in Fig. 9c. When the number of UEs grows in a single attocell, the range of variations of the access sum rate reduces, thereby lowering the chance for the downlink system to undergo a backhaul bottleneck. Fig. 9d shows that the performance of ARPC is worse than all other schemes. The use of ARPC leads to 50% BBO probability for $\lambda = 5$ UE/Cell even for a single tier super cell. For a given N_{T}, BBO is more likely when λ increases especially for $N_{\mathrm{T}} > 1$. By contrast, for a fixed value of λ, BBO is less probable when more tiers are added to the super cell. The reason for this trend is because UEs are associated with the entire branch as a whole and hence they are distributed over a larger number of attocells. This increases the probability that some attocells remain empty, which decreases the aggregate sum rate of the access system. Such a trend decays when the average UE density is sufficiently high, i.e. for $\lambda = 5$ UE/Cell.

3) Average Sum Rate Performance: To measure the end-to-end sum rate performance with power control, the bandwidth allocation ratios for an N_{T}-tier super cell are computed by applying optimal CBS based on Algorithm 2, per random realization of UEs.

Fig. 10a demonstrates the average sum rate performance for NPC, MSPC, ASPC and ARPC schemes versus N_{T} for $\lambda = 5$ UE/Cell and $B_{\mathrm{b}} = 3B_{\mathrm{a}}$. The performance of NPC is also shown as a benchmark. It can be observed that MSPC and ASPC schemes provide the same performance as NPC for all values of N_{T}. They achieve 74, 221, 442, 734 and 1083 Mbits/s, for $N_{\mathrm{T}} = 1, 2, 3, 4, 5$, respectively. Still, the average sum rate for ARPC is slightly lower than the rest of the schemes. The relative performance losses for ARPC are around 10%, 6%, 5%, 4% and 2% for $N_{\mathrm{T}} = 1, 2, 3, 4, 5$. Note that although the use of ARPC leads to high BBO probabilities as shown in Fig. 9d, it is of a less impact on the average sum rate performance. This is partly attributed to the optimal CBS algorithm which attempts to maximally approach the effective achievable sum rate of the end-to-end system. This could also be anticipated from the function of ARPC whereby the backhaul power is tuned to the average sum rate of the access system.

Fig. 10b shows $K^{*}_{\mathrm{b,min}}$ associated with each scheme for the same bandwidth of $B_{\mathrm{b}} = 3B_{\mathrm{a}}$ as used in Fig. 10a. Comparing Fig. 10b with Fig. 10a, it can be observed that remarkable power savings are attained while maintaining the average sum rate performance. For the particular case of $N_{\mathrm{T}} = 3$, by using MSPC, the backhaul system operates with only 14% of the full power limit, without affecting the average sum rate. The PE can be further improved by employing ASPC. Note that both cases of MSPC and ASPC equally have a zero BBO probability according to Fig. 8. For the case of ARPC, albeit the improvement in PE is achieved at the cost of a slight reduction in the average sum rate performance. From the PE perspective, ASPC improves upon MSPC, and at the same

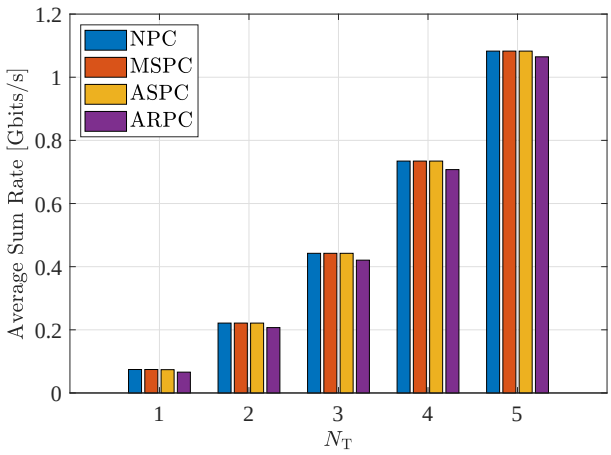

(a) Average end-to-end sum rate.

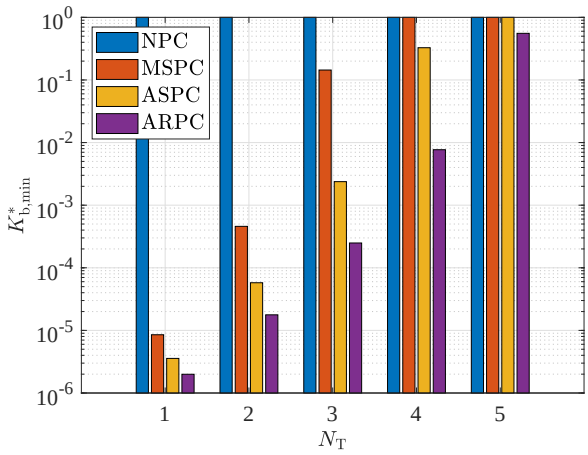

(b) Power control coefficient.

Fig. 10: The average sum rate performance for NPC, MSPC, ASPC and ARPC schemes versus the total number of tiers N_{T} for $\lambda = 5$ UE/Cell and $B_{\mathrm{b}} = 3B_{\mathrm{a}}$. The corresponding power control coefficients are shown for comparison.

time acquires a BBO performance similar to the baseline NPC scheme. This suggests that there is an optimum threshold for designing FPC-based schemes to strike a tradeoff between the total power minimization and the backhaul bottleneck minimization. The use of ARPC, though offering significant power savings, can lead to 50% BBO probability regardless of the number of tiers deployed. Such a poor performance disqualifies the impressive PE gain that is offered by ARPC in terms of the total backhaul power.

VI. Conclusions

A multi-hop wireless optical backhaul configuration is designed for multi-tier optical attocell networks in a systematic way by means of single-gateway super cells. In effect, by expanding the size of super cells, the number of gateways required to supply backhaul connectivity for a network of the same size is progressively reduced, albeit at a price. The tradeoff between the size and the end-to-end performance is underlined by numerical results. Depending on the available bandwidth and power, the backhaul rate limit becomes bottleneck if a large number of tiers is deployed. Under a low

UE density scenario, both optimal UBS and CBS algorithms cause the average sum rate performance to almost reach the maximum rate limit of the access and backhaul systems. As compared to the baseline PWF bandwidth allocation, the gain is more pronounced when the number of tiers is increased. For a high UE density, optimal CBS takes the lead, and closely realizes the overall rate limit. Furthermore, each of the proposed FPC schemes offers a PE improvement paired with a certain BBO performance. In this respect, MSPC achieves a very low BBO probability similar to the benchmark NPC scheme, while providing considerable power savings especially for fewer number of tiers. By comparison, ASPC performs better than MSPC in terms of power reduction, and maintains the same BBO probability. The use of ARPC, though delivering the best PE among the candidate schemes, leads to a substantial degradation in BBO. In addition, both MSPC and ASPC achieve an identical average sum rate performance compared to NPC, and ARPC returns a slightly less value because of underestimating the required power.

REFERENCES

[1] H. Kazemi, M. Safari, and H. Haas, "Bandwidth Scheduling and Power Control for Wireless Backhauling in Optical Attocell Networks," in *Proc. IEEE Global Commun. Conf. (GLOBECOM)*, Dec. 2018, pp. 1–7.

[2] M. Figueiredo, L. N. Alves, and C. Ribeiro, "Lighting the Wireless World: The Promise and Challenges of Visible Light Communication," *IEEE Consum. Electron. Mag.*, vol. 6, no. 4, pp. 28–37, Oct. 2017.

[3] N. Wang, E. Hossain, and V. K. Bhargava, "Backhauling 5G Small Cells: A Radio Resource Management Perspective," *IEEE Wireless Commun.*, vol. 22, no. 5, pp. 41–49, Oct. 2015.

[4] T. Koonen, "Fiber to the Home/Fiber to the Premises: What, Where, and When?" *Proc. IEEE*, vol. 94, no. 5, pp. 911–934, May 2006.

[5] W. Ni, R. P. Liu, I. B. Collings, and X. Wang, "Indoor Cooperative Small Cells over Ethernet," *IEEE Commun. Mag.*, vol. 51, no. 9, pp. 100–107, Sep. 2013.

[6] A. Papaioannou and F. Pavlidou, "Evaluation of Power Line Communication Equipment in Home Networks," *IEEE Sensors J.*, vol. 3, no. 3, pp. 288–294, Sep. 2009.

[7] C. Dehos, J. L. Gonzalez, A. D. Domenico, D. Kténas, and L. Dussopt, "Millimeter-Wave Access and Backhauling: The Solution to the Exponential Data Traffic Increase in 5G Mobile Communications Systems?" *IEEE Commun. Mag.*, vol. 52, no. 9, pp. 88–95, Sep. 2014.

[8] M. Timmers, M. Guenach, C. Nuzman, and J. Maes, "G.fast: Evolving the Copper Access Network," *IEEE Commun. Mag.*, vol. 51, no. 8, pp. 74–79, Aug. 2013.

[9] T. Komine and M. Nakagawa, "Integrated System of White LED Visible-Light Communication and Power-Line Communication," *IEEE Trans. Consum. Electron.*, vol. 49, no. 1, pp. 71–79, Feb. 2003.

[10] T. Komine, S. Haruyama, and M. Nakagawa, "Performance Evaluation of Narrowband OFDM on Integrated System of Power Line Communication and Visible Light Wireless Communication," in *Proc. IEEE 1st Int. Symp. Wireless Pervasive Comput.*, Jan. 2006.

[11] J. Song, W. Ding, F. Yang, H. Yang, B. Yu, and H. Zhang, "An Indoor Broadband Broadcasting System Based on PLC and VLC," *IEEE Trans. Broadcast.*, vol. 61, no. 2, pp. 299–308, Jun. 2015.

[12] H. Ma, L. Lampe, and S. Hranilovic, "Hybrid Visible Light and Power Line Communication for Indoor Multiuser Downlink," *IEEE/OSA J. Opt. Commun. Netw.*, vol. 9, no. 8, pp. 635–647, Aug. 2017.

[13] P. Mark, "Ethernet over Light," Master's thesis, University of British Columbia, Dec. 2014.

[14] F. Delgado, I. Quintana, J. Rufo, J. A. Rabadan, C. Quintana, and R. Perez-Jimenez, "Design and Implementation of an Ethernet-VLC Interface for Broadcast Transmissions," *IEEE Commun. Lett.*, vol. 14, no. 12, pp. 1089–1091, Dec. 2010.

[15] Y. Wang, N. Chi, Y. Wang, L. Tao, and J. Shi, "Network Architecture of a High-Speed Visible Light Communication Local Area Network," *IEEE Photon. Technol. Lett.*, vol. 27, no. 2, pp. 197–200, Jan. 2015.

[16] C. W. Chow, C. H. Yeh, Y. Liu, C. W. Hsu, and J. Y. Sung, "Network Architecture of Bidirectional Visible Light Communication and Passive Optical Network," *IEEE Photon. J.*, vol. 8, no. 3, pp. 1–7, Jun. 2016.

[17] Y. Wang, J. Shi, C. Yang, Y. Wang, and N. Chi, "Integrated 10 Gb/s multilevel multiband passive optical network and 500 Mb/s indoor visible light communication system based on Nyquist single carrier frequency domain equalization modulation," *Opt. Lett.*, vol. 39, no. 9, pp. 2576–2579, May 2014.

[18] H. Kazemi, M. Safari, and H. Haas, "A Wireless Backhaul Solution Using Visible Light Communication for Indoor Li-Fi Attocell Networks," in *Proc. IEEE Int. Conf. Commun. (ICC)*, May 2017, pp. 1–7.

[19] ——, "A Wireless Optical Backhaul Solution for Optical Attocell Networks," *IEEE Trans. Wireless Commun.*, vol. 18, no. 2, pp. 807–823, Feb. 2019.

[20] ——, "Multi-Hop Wireless Optical Backhauling for LiFi Attocell Networks: Bandwidth Scheduling and Power Control," *Preprint Version*, arXiv:1907.05967 [cs.IT], July 2019.

[21] C. Chen, D. A. Basnayaka, and H. Haas, "Downlink Performance of Optical Attocell Networks," *IEEE/OSA J. Lightw. Technol.*, vol. 34, no. 1, pp. 137–156, Jan. 2016.

[22] J. M. Kahn and J. R. Barry, "Wireless Infrared Communications," *Proc. IEEE*, vol. 85, no. 2, pp. 265–298, Feb. 1997.

[23] K. Lee, H. Park, and J. R. Barry, "Indoor Channel Characteristics for Visible Light Communications," *IEEE Commun. Lett.*, vol. 15, no. 2, pp. 217–219, Feb. 2011.

[24] T. Cover and A. E. Gamal, "Capacity Theorems for the Relay Channel," *IEEE Trans. Inf. Theory*, vol. 25, no. 5, pp. 572–584, Sep. 1979.

[25] S. Boyd and L. Vandenberghe, *Convex Optimization*. Cambridge University Press, Mar. 2004.

[26] D. P. Bertsekas, *Nonlinear Programming*, 3rd ed. Athena Scientific, 2016.

[27] S. Boyd, "Subgradient Methods," Lecture Notes for EE364b, Stanford University, May 2014.

[28] E. K. P. Chong and S. H. Zak, *An Introduction to Optimization*, 4th ed. Wiley-Interscience Publication, Feb. 2013.

[29] M. D. Soltani, X. Wu, M. Safari, and H. Haas, "Bidirectional User Throughput Maximization Based on Feedback Reduction in LiFi Networks," *IEEE Trans. Commun.*, vol. 66, no. 7, pp. 3172–3186, Jul. 2018.

[30] A. Legout, J. Nonnenmacher, and E. W. Biersack, "Bandwidth-Allocation Policies for Unicast and Multicast Flows," *IEEE/ACM Trans. Netw.*, vol. 9, no. 4, pp. 464–478, Aug. 2001.

[31] M. Vallentin, *Probability and Statistics Cookbook*, Dec. 2017, Version 0.2.6. [Online]. Available: http://statistics.zone/

[32] W. Feller, *An Introduction to Probability Theory and Its Applications*, 3rd ed. John Wiley & Sons, Inc., 1968, vol. 1.

Hossein Kazemi (Member, IEEE) received his M.Sc. degree in Electrical Engineering (Microelectronic Circuits) from Sharif University of Technology, Tehran, Iran, in 2011, and his M.Sc. degree (Hons.) in Electrical Engineering (Communication Systems) from Özyeğin University, Istanbul, Turkey, in 2014. He also received his Ph.D. degree in Electrical Engineering from the Institute for Digital Communications, University of Edinburgh, Edinburgh, UK, in 2019. He is currently a postdoctoral research associate at the LiFi Research and Development Center, University of Edinburgh. His main research interests include communication theory, wireless communications and optical wireless communications.

Majid Safari (Member, IEEE) received his Ph.D. degree in Electrical and Computer Engineering from the University of Waterloo, Canada in 2011. He also received his B.Sc. degree in Electrical and Computer Engineering from the University of Tehran, Iran, in 2003, M.Sc. degree in Electrical Engineering from Sharif University of Technology, Iran, in 2005. He is currently a senior lecturer (Associate Professor) in the Institute for Digital Communications at the University of Edinburgh. Before joining Edinburgh in 2013, He held postdoctoral fellowship at McMaster University, Canada. Dr. Safari is currently an associate editor of IEEE Transactions on Communications and was the TPC co-chair of the 4th International Workshop on Optical Wireless Communication in 2015. His main research interest is the application of information theory and signal processing in optical communications including fiber-optic communication, free-space optical communication, visible light communication, and quantum communication.

Harald Haas (Fellow, IEEE) received the Ph.D. degree from the University of Edinburgh in 2001. He is currently the Chair of Mobile Communications at The University of Edinburgh, and he is the Initiator, Co-Founder, and Chief Scientific Officer of pureLiFi Ltd., and the Director of the LiFi Research and Development Centre, The University of Edinburgh. He has authored 500 conference and journal papers. His main research interests are in optical wireless communications, hybrid optical wireless and RF communications, spatial modulation, and interference coordination in wireless networks. He is an Associate Editor of the IEEE Journal of Lightwave Technologies. He gave two TED Global talks "Wireless Data From Every light Bulb" and "Forget Wi-Fi: Meet the New Li-Fi Internet" which together have been downloaded more than 5.5 million times. In 2012 and 2017, he was a recipient of the prestigious Established Career Fellowship from the Engineering and Physical Sciences Research Council (EPSRC) in the U.K. In 2014, he was selected by EPSRC as one of ten Recognizing Inspirational Scientists and Engineers Leaders in the U.K. He was a co-recipient of the EURASIP Best Paper Award for the Journal on Wireless Communications and Networking in 2015 and the Jack Neubauer Memorial Award of the IEEE Vehicular Technology Society. In 2016, he received the Outstanding Achievement Award from the International Solid State Lighting Alliance. He was a co-recipient of recent best paper awards at VTC-Fall, 2013, VTC-Spring 2015, ICC 2016, ICC 2017 and ICC 2018. In 2019 he received the James Evans Avant Garde Award of the IEEE Vehicular Technology Society. Haas is a Fellow of the Royal Academy of Engineering.